

Goal-Oriented Adaptive THB-Spline Schemes for PDE-Based Planar Parameterization

Jochen Hinz^{a,*}, Michael Abdelmalik^{b,*}, Matthias Möller^a,

^aDepartment of Applied Mathematics

Delft University of Technology, 2628 XE Delft, Netherlands

^bOden Institute, University of Texas at Austin, 78712 Austin, Texas, US

Abstract

This paper presents a PDE-based planar parameterization framework with support for *Truncated Hierarchical B-Splines* (THB-splines). For this, we adopt the a posteriori refinement strategy of *Dual Weighted Residual* and present several adaptive numerical schemes for the purpose of approximating an inversely harmonic geometry parameterization. Hereby, the combination of goal-oriented a posteriori strategies and THB-enabled local refinement avoids over-refinement, in particular in geometries with complex boundaries. To control the parametric properties of the outcome, we introduce the concept of domain refinement. Hereby, the properties of the domain into which the mapping maps inversely harmonically, are optimized in order to fine-tune the parametric properties of the recomputed geometry parameterization.

Keywords: Parameterization Techniques, Isogeometric Analysis, THB-splines, Elliptic Grid Generation, Dual Weighted Residual, Shape Optimization

1. Introduction

Isogeometric analysis (IGA), first introduced by Hughes et al. in [1], is a numerical technique that aims to bridge the gap between computer aided design (CAD) and (isoparametric) finite element analysis (FEA). This is accomplished by building the geometry mapping from the same spline basis that is used to approximately solve PDE-problems posed over the geometry. As such, spline-based parameterization techniques have received an increased amount of interest in the mathematical community in recent years. Since the CAD pipeline typically provides no more than a spline-based description of the boundary contours of the target geometry, the purpose of all parameterization algorithms is to generate a bijective (folding-free) geometry parameterization from the boundary CAD data. Analogous to mesh quality in classical FEA, the parametric quality of the surface parameterization has a profound impact on the numerical accuracy of the isogeometric analysis [2]. Therefore, besides bijectivity, proficient parameterization algorithms aim at generating parameterizations of high numerical quality.

One of the most important applications of IGA lies in shape-optimization problems. Since the geometry changes at every shape optimization iteration, algorithms that are differentiable with respect to the design variables (i.e., the boundary control points) have a further advantage since they allow for employing gradient-based shape-optimization algorithms which tend to converge in fewer iterations than their zeroth-order counterparts. Another advantage of differentiability is efficiency: as the inner control points are a smooth function of the boundary control points, there is no need for full remeshing after each iteration since cheaper mesh update strategies can be employed. This is also true for settings in which the boundary contours

*Corresponding author

Email addresses: j.p.hinz@tudelft.nl (Jochen Hinz), M.Abdel.Malik@tue.nl (Michael Abdelmalik), m.moller@tudelft.nl (Matthias Möller)

change as a smooth function of time.

Traditionally, parameterizations for IGA-applications are built from tensor-product spline spaces. Unfortunately, structured spline technologies do not allow for local refinement as knot-insertion in one parametric direction automatically refines a whole row / column of the underlying spline space. For the geometry description, this may result in a very dense spline basis whenever many degrees of freedom (DOFs) are required to properly resolve the boundary contours. As a result, the total number of unknowns (the inner control points) may become infeasibly large, leading to a severe slow-down of the meshing process and / or the isogeometric analysis.

To address above efficiency concerns, this paper introduces a PDE-based planar parameterization framework that uses THB-splines [3], an unstructured spline-technology which allows for local refinement, potentially reducing the required total number of DOFs. A major challenge of unstructured spline technologies is deciding where local refinement is required and where a lower resolution suffices. For this, we employ the principles of *dual weighted residual* (DWR) [4], an a posteriori refinement technique for PDE-problems based on duality considerations. Furthermore, we augment the problem formulation with a mechanism that allows for changing the parametric properties of the PDE-solution in order to fine-tune the parametric properties of the mapping operator.

1.1. Notation

In this work, we denote vectors in boldface. The i -th entry of vector \mathbf{x} is denoted by x_i or simply x_i and similarly for the ij -th entry of matrices. We make extensive use of vector derivatives. Here, we interchangeably use the denotation

$$\partial_t \mathbf{x} \equiv \frac{\partial \mathbf{x}}{\partial t}, \quad \text{with} \quad \left[\frac{\partial \mathbf{x}}{\partial t} \right]_{ij} = \frac{\partial x_i}{\partial t_j} \quad (1)$$

for the partial derivative.

1.2. THB-Splines

In the following we give a brief discussion of the concept of Truncated Hierarchical B-splines (THB-splines). THB-splines, first introduced in [5], is an unstructured spline technology which extends the concept of Hierarchical B-splines (HB-splines) [6] by restoring the partition of unit property which does not hold in a HB-setting.

Let $\hat{\mathcal{V}}_h^0 = \{w_1^0, \dots, w_n^0\}$ be a structured B-spline basis. By $\hat{\mathcal{V}}_h^i \supset \hat{\mathcal{V}}_h^0$, we denote the basis acquired upon performing uniform h -refinement on $\hat{\mathcal{V}}_h^0$ a total of i times. Let T^i denote the matrix that prolongs the vector of weights \mathbf{c}^i corresponding to some $u \in \hat{\mathcal{V}}_h^i$ to $\hat{\mathcal{V}}_h^{i+1}$. The prolonged \mathbf{c}^{i+1} is then given by $\mathbf{c}^{i+1} = T^i \mathbf{c}^i$. Given some basis \mathcal{V}_h , with $\mathcal{V}_h = \hat{\mathcal{V}}_h^0$ initially, in traditional HB-splines, local refinement is accomplished by marking some $w_i^0 \in \mathcal{V}_h$ for refinement and replacing its supporting elements by their finer counterparts from the element hierarchy. Next, w_i^0 is removed and replaced by

$$\{w_i^0\} \rightarrow \{w_j^1 \in \hat{\mathcal{V}}_h^1 \mid T_{i,j}^0 \neq 0\}, \quad \text{in } \mathcal{V}_h. \quad (2)$$

This operation may then be performed repeatedly, leading to a basis and corresponding element segmentation comprised of basis functions and elements from several levels in the hierarchy. Unfortunately, the partition of unity property associated with \mathcal{V}_h is lost upon HB-refinement. To remedy this, [5] propose accompanying the replacement in (2) by a truncation of the remaining $w_j^0 \in \mathcal{V}_h$. Note that for every $w_j^0 \in \mathcal{V}_h$ we can write

$$w_j^0 = \sum_k T_{j,k}^0 w_k^1. \quad (3)$$

Therefore, along with (2), THB-refinement replaces $w_j^0 \rightarrow w_j^0 - T_{j,k}^0 w_k^1$ in \mathcal{V}_h if $T_{i,k}^0 \neq 0$ in $w_i^0 = \sum_k T_{i,k}^0 w_k^1$, and similarly for repeated refinements. By accompanying refinement with truncation, the partition of unity

property is restored. For more details, we refer to [5].

For the purpose of this work it is sufficient to note that, since refinement of single elements may have no effect on \mathcal{V}_h , refinement always removes at least one basis function from \mathcal{V}_h while replacing all supporting elements by their finer counterparts. Refinement is hence less local than in a classical FEM setting but sufficiently local in practice.

1.3. Problem Statement

In this section we will give a general formulation of the problem considered in this work.

Let Ω denote the target geometry and let $\hat{\Omega} = [0, 1]^2$ denote the domain. In general, we assume that Ω is topologically equivalent to $\hat{\Omega}$. By $\mathbf{x} : \hat{\Omega} \rightarrow \Omega$, we denote the mapping operator that we attempt to build from the linear span of the (THB-)spline basis $\mathcal{V}_h = \{w_1, \dots, w_N\}$. The mapping operator $\mathbf{x} : \hat{\Omega} \rightarrow \Omega$ is of the form:

$$\mathbf{x}(\xi, \eta) = \sum_{i \in \mathcal{I}_{\text{boundary}}} \mathbf{c}_i w_i(\xi, \eta) + \sum_{j \in \mathcal{I}_{\text{inner}}} \mathbf{c}_j w_j(\xi, \eta), \quad (4)$$

where $\mathcal{I}_{\text{inner}}$ and $\mathcal{I}_{\text{boundary}}$ refer to the index-sets corresponding to vanishing and nonvanishing basis functions on $\partial\hat{\Omega}$, respectively. Note that $\mathcal{I}_{\text{inner}}$ and $\mathcal{I}_{\text{boundary}}$ are mutually disjoint and

$$\mathcal{I}_{\text{inner}} \cup \mathcal{I}_{\text{boundary}} = \{1, \dots, N\}.$$

In general, we assume that

$$\partial\Omega \in \text{span } \mathcal{V}_h|_{\partial\hat{\Omega}}^2$$

and that the \mathbf{c}_i in (4) are chosen such that $\mathbf{x}|_{\hat{\Omega}}$ is a Jordan curve that parameterizes $\partial\Omega$. The purpose of any parameterization algorithm is then to choose the \mathbf{c}_j in (4) such that

1. $\mathbf{x} : \hat{\Omega} \rightarrow \Omega$ is bijective,
2. \mathbf{x} is a parameterization of high numerical quality,

while the \mathbf{c}_i are typically held fixed.

1.4. Related Work

Existing parameterization techniques can be divided into three broad categories:

1. algebraic (direct) methods;
2. methods based on (constrained and unconstrained) quality cost function optimization;
3. PDE-based methods.

Algebraic methods (1.) generate a mapping from the solution of a linear system of equations or the evaluation of a closed-form expression. The most-widely used algebraic method is based on the Coon's patch approach [7]. Given the four (known) boundary curves $\mathbf{x}(\xi, 0)$, $\mathbf{x}(1, \eta)$, $\mathbf{x}(\xi, 1)$ and $\mathbf{x}(0, \eta)$, the mapping is constructed by projecting the components of

$$\begin{aligned} \mathbf{x}_{\text{Coons}} &= (1 - \xi)\mathbf{x}(0, \eta) + \xi\mathbf{x}(1, \eta) \\ &\quad + (1 - \eta)\mathbf{x}(\xi, 0) + \eta\mathbf{x}(\xi, 1) \\ &\quad - \begin{bmatrix} 1 - \xi & \xi \end{bmatrix} \begin{bmatrix} \mathbf{x}(0, 0) & \mathbf{x}(0, 1) \\ \mathbf{x}(1, 0) & \mathbf{x}(1, 1) \end{bmatrix} \begin{bmatrix} 1 - \eta \\ \eta \end{bmatrix} \end{aligned} \quad (5)$$

onto the spline space \mathcal{V}_h . Whenever \mathcal{V}_h is a tensor-product spline basis, the inner control points can also be computationally inexpensively computed from an explicit formula, see [7], while in an unstructured setting equation (5) can be used.

Another class of algebraic methods results from minimizing a convex, quadratic cost function $Q(\mathbf{x})$ over the

inner control points $\mathbf{c}_j, j \in I_{\text{inner}}$. As before, the boundary control points follow from the boundary contours and are held fixed. $Q(\mathbf{x})$ is typically given by a positively-weighted sum of several cost functions. As such, it takes the form:

$$Q(\mathbf{x}) = \sum_i \underbrace{\lambda_i}_{\geq 0} Q_i(\mathbf{x}), \quad (6)$$

while the minimization problem becomes:

$$\int_{\hat{\Omega}} Q(\mathbf{x}) dS \rightarrow \min_{\mathbf{x} \in \mathcal{V}_h^2}, \quad \text{s.t. } \mathbf{x}|_{\partial\hat{\Omega}} = \partial\Omega. \quad (7)$$

Possible choices for the $Q_i(\mathbf{x})$ in (6) are [5]:

$$Q_{\text{length}}(\mathbf{x}) = \|\mathbf{x}_{\xi}\|^2 + \|\mathbf{x}_{\eta}\|^2 \quad \text{and} \quad Q_{\text{uniformity}}(\mathbf{x}) = \|\mathbf{x}_{\xi\xi}\|^2 + 2\|\mathbf{x}_{\xi\eta}\|^2 + \|\mathbf{x}_{\eta\eta}\|^2, \quad (8)$$

where the latter requires global C^1 -continuity of the spline basis \mathcal{V}_h . The minimization of (7) converges after one iteration of a Newton-type optimization algorithm and can hence be considered of type (1.) as well as type (2.). For an overview of type (1.) approaches, we refer to [8].

Another convex but quartic cost function is the *Liao*-functional [9]

$$Q_{\text{Liao}} = g_{11}^2 + 2g_{12}^2 + g_{22}^2, \quad (9)$$

where the g_{ij} denote the entries of the metric tensor G of the mapping, with

$$g_{ij} = \mathbf{x}_{\xi_i} \cdot \mathbf{x}_{\xi_j} \quad \text{and} \quad \xi = (\xi, \eta)^T. \quad (10)$$

The minimization of above cost functions is computationally efficient, thanks to convexity, however, the resulting mappings are often folded, i.e., they do not satisfy:

$$\det J > 0, \quad \forall (\xi, \eta) \in \hat{\Omega}, \quad (11)$$

where J denotes the Jacobian determinant of \mathbf{x} .

The minimization of nonconvex quality functionals is computationally more demanding but tends to yield better results in cases where convex optimization leads to a folded mapping [9]. Typical nonconvex quality functionals are:

- the *area* functional

$$Q_{\text{area}} = \det J^2, \quad (12)$$

which aims at minimizing the variance of $\det J$ over $\hat{\Omega}$;

- the *orthogonality* functional

$$Q_{\text{Orthogonality}} = g_{12}^2 \quad \text{or} \quad Q_{\text{AreaOrthogonality}} = g_{11}g_{22}, \quad (13)$$

which is aimed at orthogonalizing the parameter lines;

- the *eccentricity* functional

$$Q_{\text{eccen}} = \left(\frac{\mathbf{x}_{\xi} \cdot \mathbf{x}_{\xi\xi}}{g_{11}} \right)^2 + \left(\frac{\mathbf{x}_{\eta} \cdot \mathbf{x}_{\eta\eta}}{g_{22}} \right)^2, \quad (14)$$

which penalizes fast accelerations along the parameter lines.

Unfortunately, minimization of the above functionals, in many cases, leads to folding, too. To the best of our knowledge, there are two main ways to prevent the grid from folding:

- (a) penalization;
- (b) constrained minimization.

Option (a) attempts to prevent grid folding through the modification of existing cost functions with a penalty term, such as

- the *Modified Liao* functional

$$Q_{\text{ML}} = \left(\frac{g_{11} + g_{22}}{\det J} \right)^2. \quad (15)$$

Adding the Jacobian determinant in the denominator serves the purpose of mitigating the tendency to fold, since the cost functional possesses an infinite barrier close to the boundary of the feasible region. The most widely-used penalty cost functional is the so-called

- *Winslow* functional

$$Q_{\text{W}} = \frac{g_{11} + g_{22}}{\det J}. \quad (16)$$

The *Winslow* functional (16) follows from performing a pullback of the problem

$$\int_{\Omega} \|\xi_x\|^2 + \|\xi_y\|^2 dx \rightarrow \min_x, \quad \text{s.t.} \quad \xi|_{\partial\Omega} = \partial\hat{\Omega} \quad (17)$$

into $\hat{\Omega}$. An approach based on the *Winslow* functional can be regarded as the *inverse mapping* counterpart of an approach based on the *length functional* (8).

In option (b), the minimization is carried out with an added constraint that constitutes a sufficient condition for (11). For tensor-product B-spline bases, in [10], Xu et al. propose a linear convex sufficient condition $L(\mathbf{x}) > 0$ for bijectivity. It is added as a constraint to the minimization problem. If convex cost functions are utilized, this leads to a linear programming problem, which can be computationally inexpensively solved using convex optimization routines. Unfortunately, the set

$$\{\mathbf{x} \in \text{span } \mathcal{V}_h^2 \mid \mathbf{x}|_{\partial\hat{\Omega}} = \partial\Omega \text{ and } L(\mathbf{x}) > 0\}$$

may be empty or the constraint may be very restrictive, limiting its applicability to relatively simple shapes. In an effort to allow for more complicated shapes, [10] and [8] propose nonlinear nonconvex sufficient conditions for bijectivity. Since the Jacobian determinant $\det J$ is a piecewise-polynomial function of higher polynomial degree itself, it can be projected onto a spline basis that contains it. If all the weights are positive under the expansion, this constitutes a sufficient condition for bijectivity. The nonlinear sufficient condition $N(\mathbf{x}) > 0$ is added as a constraint and the optimization is carried out with a black box nonlinear optimization routine (typically, IPOPT [11]) that comes with all the drawbacks of nonconvex optimization such as the danger of getting stuck in local minima. A further disadvantage is the need for an initial guess that satisfies the constraints, for which another nonconvex optimization problem has to be solved first.

While the extension of (penalized or unpenalized) cost function minimization to THB-splines is straightforward, this is not the case for constrained methods, since the constraints are designed for structured splines only. To the best of our knowledge, the only comprehensive overview of planar parameterization techniques for THB-splines can be found in [5], where the application of most of the mentioned (unpenalized) cost functions is studied in a THB-setting. As the optimization is carried out without constraints, folding occurs in the majority of test cases. The paper concludes that the only method potentially capable of dealing with

arbitrarily-complex shapes is based on computing \mathbf{x} by approximating the inverse of a map \mathbf{h} which is comprised of a pair of harmonic functions on Ω , i.e.,

$$\Delta \mathbf{h} = \mathbf{0} \quad \text{in } \Omega, \quad \text{s.t.} \quad \mathbf{h}|_{\partial\Omega} = \partial\hat{\Omega}. \quad (18)$$

The authors propose a two-step approach: First a large number of tuples $(\mathbf{h}(\mathbf{x}_j), \mathbf{x}_j)$, with $\mathbf{x}_j \in \Omega$ is computed using an isogeometric boundary element method [12, 13], after which the pairs are utilized to approximate \mathbf{h}^{-1} through a least-squares minimization problem with regularization terms.

Above methodology is equivalent to minimizing the *Winslow* functional (16), which follows straightforwardly from deriving the Euler-Lagrange equations of the minimization problem (17). As \mathbf{h} is a pair of harmonic functions with convex target domain, it follows from the Radó-Kneser-Choquet theorem that \mathbf{h} is a diffeomorphism in the interior of Ω [8], justifying an approximation of its inverse for the purpose of computing a domain parameterization.

A major advantage of the two-step approach from [5] over a direct minimization of (16) is that the latter requires a folding-free initial domain parameterization to avoid division by zero. In the vast majority of cases, however, such a bijection is not available, limiting its applicability to improving the parametric properties of an already bijective mapping.

An advantage of minimizing (16), however, is that if the global minimum over $\text{span } \mathcal{V}_h^2$ has been found, it is clearly bijective, while bijectivity may be lost in the indirect approach, due to numerical inaccuracies.

The observation that the impractical minimization of the *Winslow* functional (16) is equivalent to solving an inverse Laplace problem has lead to the development of (3.) PDE-based parameterization methods. To acquire a PDE-problem posed over $\hat{\Omega}$, we perform a pullback:

$$\Delta_{\mathbf{x}} \xi = \mathbf{0} \quad \text{in } \hat{\Omega}, \quad \text{s.t.} \quad \mathbf{x}|_{\partial\hat{\Omega}} = \partial\Omega, \quad (19)$$

where $\Delta_{\mathbf{x}}$ denotes the Laplace-Beltrami [14] operator with respect to Ω . Problem (19) suffers from the same shortcoming of the *Winslow*-approach: the appearance of a Jacobian determinant in the denominator. However, we may scale the equation by multiplying with any nonsingular 2×2 tensor T . Choosing $T = (\det \mathbf{x}_{\xi})^2 \mathbf{x}_{\xi}$ (which is nonsingular thanks to the bijectivity of the PDE-solution), the Jacobian-determinant can be removed from (19), leading to the following quasi-linear second-order PDE-problem [15]:

$$A(\mathbf{x}): H(x_i) = 0 \quad \text{in } \hat{\Omega}, \quad \text{for } i \in \{1, 2\} \quad \text{s.t.} \quad \mathbf{x}|_{\partial\hat{\Omega}} = \partial\Omega, \quad (20)$$

where

$$H(u)_{ij} = \frac{\partial^2 u}{\partial \xi_i \partial \xi_j} \quad \text{and} \quad A(\mathbf{x}) = \frac{1}{g_{11} + g_{22} + \epsilon} \begin{pmatrix} g_{22} & -g_{12} \\ -g_{12} & g_{11} \end{pmatrix}, \quad (21)$$

with the g_{ij} as in (10) and ϵ a small positive constant that serves numerical stability (typically, $\epsilon \simeq 10^{-4}$). Furthermore, $A: B$ denotes the Frobenius inner product.

Remark. The purpose of dividing by $g_{11} + g_{22} + \epsilon$ in (21) is achieving scaling invariance.

In [16], equation (20) is discretized with a Galerkin approach. The resulting equations are tackled with a Newton-based iterative approach, which is initialized with an algebraic initial guess.

The advantages and disadvantages of solving (20) over a direct minimization of (16) are the same as in the indirect approach from [5]. Hence, folding resulting from insufficient numerical accuracy can be resolved by refining the basis and recomputing the mapping.

In this work, we will present several schemes for approximately solving (20) with THB spline bases. A major challenge in a THB-setting is deciding where a high resolution is needed. Since the approach is PDE-based, we adopt the a posteriori refinement strategy of *dual weighted residual*, which is the topic of Section 3.1.

2. Solution Strategies

In this section we present several solution strategies to approximately solve (20). As the resulting equations are nonlinear, we base our solution strategy on iterative approaches. Initial guesses are always constructed using an algebraic method (see Section 1).

Let $\mathcal{V}^f = \{\mathbf{v} \in \mathcal{V}^2 \mid \mathbf{v} = \mathbf{f} \text{ on } \partial\hat{\Omega}\}$ and let \mathcal{V}_h^f be the subspace resulting from replacing \mathcal{V} by the finite-dimensional $\mathcal{V}_h \subset \mathcal{V}$. Furthermore, let \mathbf{x}_D be such that $\mathbf{x}_D|_{\partial\hat{\Omega}}$ parameterizes $\partial\Omega$ (for convenience we assume that $\mathbf{x}_D \in \mathcal{V}_h^2$).

In an IGA-setting, (20) suggests a discretization of the form:

$$\text{find } \mathbf{x}_h \in \mathcal{V}_h^{\mathbf{x}_D} \quad \text{s.t.} \quad F(\mathbf{x}_h, \boldsymbol{\sigma}_h) = 0 \quad \forall \boldsymbol{\sigma}_h \in \mathcal{V}_h^0, \quad (22)$$

with

$$F(\mathbf{x}, \boldsymbol{\sigma}) = \int_{\hat{\Omega}} \sigma_i A(\mathbf{x}) : H(\mathbf{x}_i) dS, \quad (23)$$

where we have made use of Einstein notation. As second order derivatives appear in (23), we choose $\mathcal{V} = H^2(\hat{\Omega})$.

2.1. Newton Approach

In the following, we briefly recapitulate the approach from [16], which is designated for tensor-product NURBS bases but can also be applied in a THB-setting. By

$$B'(u, \dots, z) \equiv \left. \frac{\partial B(u + \epsilon z, \dots)}{\partial \epsilon} \right|_{\epsilon=0}, \quad (24)$$

we denote the Gateaux derivative of any differentiable form $B(\cdot, \dots)$ with respect to its first argument. Given $\mathbf{x}^k \in \mathcal{V}_h^{\mathbf{x}_D}$, we compute the Newton increment from

$$\text{find } \delta \mathbf{x}^k \in \mathcal{V}_h^0 \quad \text{s.t.} \quad F'(\mathbf{x}^k, \boldsymbol{\sigma}_h, \delta \mathbf{x}^k) = -F(\mathbf{x}^k, \boldsymbol{\sigma}_h), \quad \forall \boldsymbol{\sigma}_h \in \mathcal{V}_h^0. \quad (25)$$

Upon completion, we update $\mathbf{x}^{k+1} = \mathbf{x}^k + \kappa \delta \mathbf{x}^k$ for some $\kappa \in (0, 1]$, whose optimal value is estimated using a line search routine. Above steps are repeated until the residual norm is deemed sufficiently small.

Optionally, derivative evaluations of the form $F'(\mathbf{x}^k, \boldsymbol{\sigma}_h, \mathbf{v})$ may be approximated using finite differences:

$$F'(\mathbf{x}^k, \boldsymbol{\sigma}_h, \mathbf{v}) \simeq \frac{F(\mathbf{x}^k + \epsilon \mathbf{v}, \boldsymbol{\sigma}_h) - F(\mathbf{x}^k, \boldsymbol{\sigma}_h)}{\epsilon}, \quad (26)$$

for ϵ small. Solving (25) using a suitable Krylov-subspace method only requires computing derivative evaluations $F'(\mathbf{x}^k, \boldsymbol{\sigma}_h, \mathbf{v})$, which may be approximated using (26), leading to a Newton-Krylov algorithm that avoids the expensive assembly of the Jacobian $\partial F(\mathbf{x}^k)_{ij} = F(\mathbf{x}^k, \boldsymbol{\sigma}_i, \boldsymbol{\sigma}_j)$. The optimal choice of ϵ in (26) is discussed in [17].

2.2. Pseudo-Transient Continuation

In this technique, we seek the steady-state solution of the problem

$$\text{find } \mathbf{x}_h \in \mathcal{V}_h^{\mathbf{x}_D} \times \mathbb{R}^+, \quad \text{s.t.} \quad \langle \partial_t \mathbf{x}_h, \boldsymbol{\sigma}_h \rangle = -F(\mathbf{x}_h, \boldsymbol{\sigma}_h), \quad \forall \boldsymbol{\sigma}_h \in \mathcal{V}_h^0, \quad \text{with} \quad \langle \partial_t \mathbf{x}_h, \boldsymbol{\sigma}_h \rangle = \int_{\hat{\Omega}} \boldsymbol{\sigma}_h \cdot \partial_t \mathbf{x}_h dS. \quad (27)$$

We discretize in time using backward Euler. Introducing $\delta \mathbf{x}^k = \mathbf{x}^{k+1} - \mathbf{x}^k$, with $F(\mathbf{x}^{k+1}, \boldsymbol{\sigma}_h) \simeq F(\mathbf{x}^k, \boldsymbol{\sigma}_h) + F'(\mathbf{x}^k, \boldsymbol{\sigma}_h, \delta \mathbf{x}^k)$, we compute the temporal increment from

$$\text{find } \delta \mathbf{x}^k \in \mathcal{V}_h^0 \quad \text{s.t.} \quad \left\langle \frac{\delta \mathbf{x}^k}{\delta t^k}, \boldsymbol{\sigma}_h \right\rangle + F'(\mathbf{x}^k, \boldsymbol{\sigma}_h, \delta \mathbf{x}^k) = -F(\mathbf{x}^k, \boldsymbol{\sigma}_h), \quad \forall \boldsymbol{\sigma}_h \in \mathcal{V}_h^0, \quad (28)$$

where δt^k denotes the time-step during the k -th iteration. As proposed in [18], we base the time-step selection on the following recursive formula

$$\delta t^k = \delta t^{k-1} \frac{\|\mathbf{F}(\mathbf{x}^{k-1})\|}{\|\mathbf{F}(\mathbf{x}^k)\|}, \quad \text{with} \quad \|\mathbf{F}(\mathbf{x})\|^2 = \sum_{\sigma_h \in \mathcal{V}_0^h} F(\mathbf{x}, \sigma_h)^2. \quad (29)$$

The iteration is terminated once $\|\mathbf{x}^k - \mathbf{x}^{k-1}\|$ is sufficiently small.

2.3. Picard Iteration

In the following, we present a Picard-based iterative scheme that is loosely based on the default approach from the rich literature of classical meshing techniques [19]. As opposed to subsections 2.1 and 2.2, we base the scheme on a linearize then discretize approach, rather than the converse.

Note that for given $\mathbf{x} = (x, y)^T$, we have

$$A(\mathbf{x}) = C^T(\mathbf{x})C(\mathbf{x}), \quad \text{with} \quad C(\mathbf{x}) = \frac{1}{\sqrt{g_{11} + g_{22} + \epsilon}} \begin{pmatrix} \frac{\partial y}{\partial \eta} & -\frac{\partial y}{\partial \xi} \\ -\frac{\partial x}{\partial \eta} & \frac{\partial x}{\partial \xi} \end{pmatrix}. \quad (30)$$

As such, $A(\mathbf{x})$ is symmetric positive semi-definite (SPSD) for all \mathbf{x} and symmetric positive definite (SPD) for $\mathbf{x} : \hat{\Omega} \rightarrow \Omega$ bijective. Let us introduce the operator $\mathbf{K} : C^2(\hat{\Omega}, \mathbb{R}^2) \times C^2(\hat{\Omega}, \mathbb{R}^2) \times \mathbb{R}^+ \rightarrow C^0(\hat{\Omega}, \mathbb{R}^2)$ that reads

$$\mathbf{K}_i(\mathbf{x}, \mathbf{y}, \mu) = A_\mu(\mathbf{y}) : H(\mathbf{x}_i) - \mu \Delta_\xi \mathbf{y}_i, \quad \text{with} \quad A_\mu(\mathbf{y}) = A(\mathbf{y}) + \mu I_{2 \times 2}. \quad (31)$$

Note that for $\mu > 0$, $A_\mu(\mathbf{x})$ is SPD and $\mathbf{K}_i(\mathbf{x}, \mathbf{x}, \mu) = A(\mathbf{x}) : H(\mathbf{x}_i)$. For given μ , we seek \mathbf{x} as the limit $k \rightarrow \infty$ of the recursive sequence

$$\text{find } \mathbf{x}^{k+1} \quad \text{s.t.} \quad \mathbf{K}(\mathbf{x}^{k+1}, \mathbf{x}^k, \mu) = \mathbf{0}, \quad \text{and} \quad \mathbf{x}^{k+1} = \mathbf{x}_D \quad \text{on} \quad \partial \hat{\Omega}. \quad (32)$$

To discretize (32), let us introduce the semi-linear form $G_\tau : \mathcal{V}^2 \times \mathcal{V}^2 \times \mathbb{R}^+ \times \mathcal{V}^0 \rightarrow \mathbb{R}$ with

$$G_\tau(\mathbf{x}, \mathbf{y}, \mu, \sigma) = \int_{\hat{\Omega}} \tau_i(\sigma, \mathbf{y}) A(\mathbf{y})_\mu : H(\mathbf{x}_i) dS - \mu \int_{\hat{\Omega}} \tau_i(\sigma, \mathbf{y}) \Delta_\xi \mathbf{y}_i dS, \quad (33)$$

where $\tau : \mathcal{V}^0 \times \mathcal{V}^2 \rightarrow L_2(\hat{\Omega}, \mathbb{R}^2)$ is an operator acting on the test space.

Given \mathbf{x}^k , we compute $\mathbf{x}^{k+1} \in \mathcal{V}^{\mathbf{x}_D}$ as the solution of

$$\text{find } \mathbf{x}^{k+1} \in \mathcal{V}^{\mathbf{x}_D} \quad \text{s.t.} \quad G_\tau(\mathbf{x}^{k+1}, \mathbf{x}^k, \mu, \sigma) = 0, \quad \forall \sigma \in \mathcal{V}^0, \quad (34)$$

where, as before, $\mathcal{V}^{\mathbf{x}_D} = \{\mathbf{v} \in \mathcal{V}^2 \mid \mathbf{v} = \mathbf{x}_D \text{ on } \partial \hat{\Omega}\}$.

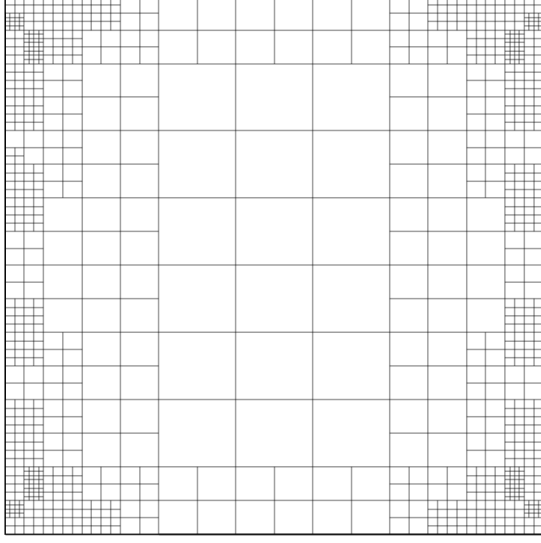
The discretization of (34) follows straightforwardly from replacing \mathcal{V} by the finite dimensional $\mathcal{V}_h \subset \mathcal{V}$. Equation (34) leads to a decoupled (block-diagonal) system of elliptic equations in nonvariational (or non-divergence) form [20]. Inspired by [21], here we consider the choices

$$\tau^{\text{Id}}(\sigma, \mathbf{y}) = \sigma, \quad \tau^{\text{div}}(\sigma, \mathbf{y}) = \gamma(\mathbf{y}) \Delta_\xi \sigma \quad \text{and} \quad \tau_i^{\text{ls}}(\sigma, \mathbf{y}) = A_\mu(\mathbf{y}) : H(\sigma_i), \quad (35)$$

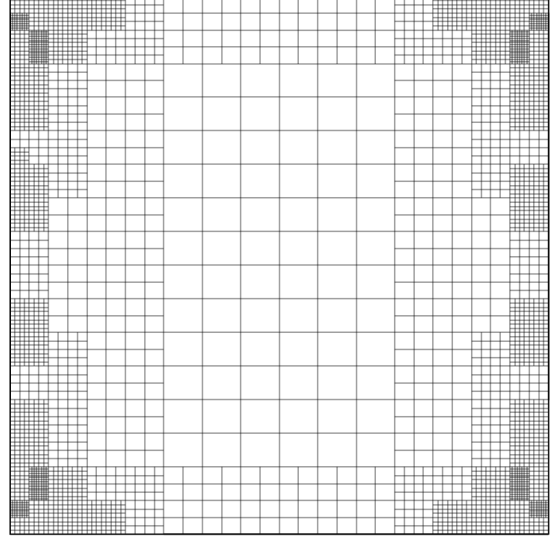
where

$$\gamma(\mathbf{y}) = \frac{\text{tr}(A_\mu(\mathbf{y}))}{A_\mu : A_\mu(\mathbf{y})}. \quad (36)$$

A Picard scheme results from iterating on (34) until $\|\mathbf{x}^{k+1} - \mathbf{x}^k\|$ is negligibly small. For all choices of τ , the Picard iteration is aimed at finding the root corresponding to the residual $F_\tau(\mathbf{x}, \sigma) = F(\mathbf{x}, \tau(\sigma, \mathbf{x}))$ (see equation (23)).



(a) The unrefined domain.



(b) The uniformly refined domain.

Figure 1: The domains used in the computations of the parameterizations from Figures 2 and 3.

refinement \ method	Direct	$\tau = \tau^{\text{ld}}$	$\tau = \tau^{\text{ls}}$	$\tau = \tau^{\text{div}}$
h	4.784	4.849	4.913	4.974
$h/2$		4.787	4.790	4.815

Table 1: Evaluation of the Winslow functional with the various parameterizations.

2.4. Direct Approach

Assuming a bijective initial guess $\mathbf{x}^0 \in \mathcal{V}_h^{\mathbf{x}_D}$ is available, we may alternatively compute and approximately inversely harmonic parameterization by a direct minimization of the Winslow functional (16). Let

$$L_W(\mathbf{x}) = \int_{\Omega} Q_W(\mathbf{x}) dS \quad (37)$$

denote the evaluation of the Winslow function (see equation (16)), whose domain is the set of all bijective \mathbf{x} . To conform with the topic of this manuscript, we compute the minimizer over $\mathcal{V}_h^{\mathbf{x}_D}$ as the solution of the following discretized PDE-problem:

$$\text{find } \mathbf{x}_h \in \mathcal{V}_h^{\mathbf{x}_D} \quad \text{s.t.} \quad L'_W(\mathbf{x}_h, \sigma_h) = 0, \quad \forall \sigma_h \in \mathcal{V}_h^0. \quad (38)$$

We solve (38) with one of the approaches from Subsections 2.1 and 2.2. Typically \mathbf{x}^0 is the solution of one of the indirect methods presented in Subsections 2.1 to 2.3. In practice, we have often encountered convergence failure even when \mathbf{x}^0 is bijective. As a rule of thumb, we retry solving (38) with a refined \mathbf{x}^0 , resulting from an indirect approach, if converge is not reached after a few iterations.

Remark. If a measure of quality of the solution results from substituting into (37), a direct approach yields the best outcome.

2.5. Example: Puzzle Piece

Figure 2 shows the various parameterizations of a puzzle piece geometry, resulting from solving the discretized equations with the different proposed methods. All methods lead to a bijective outcome.

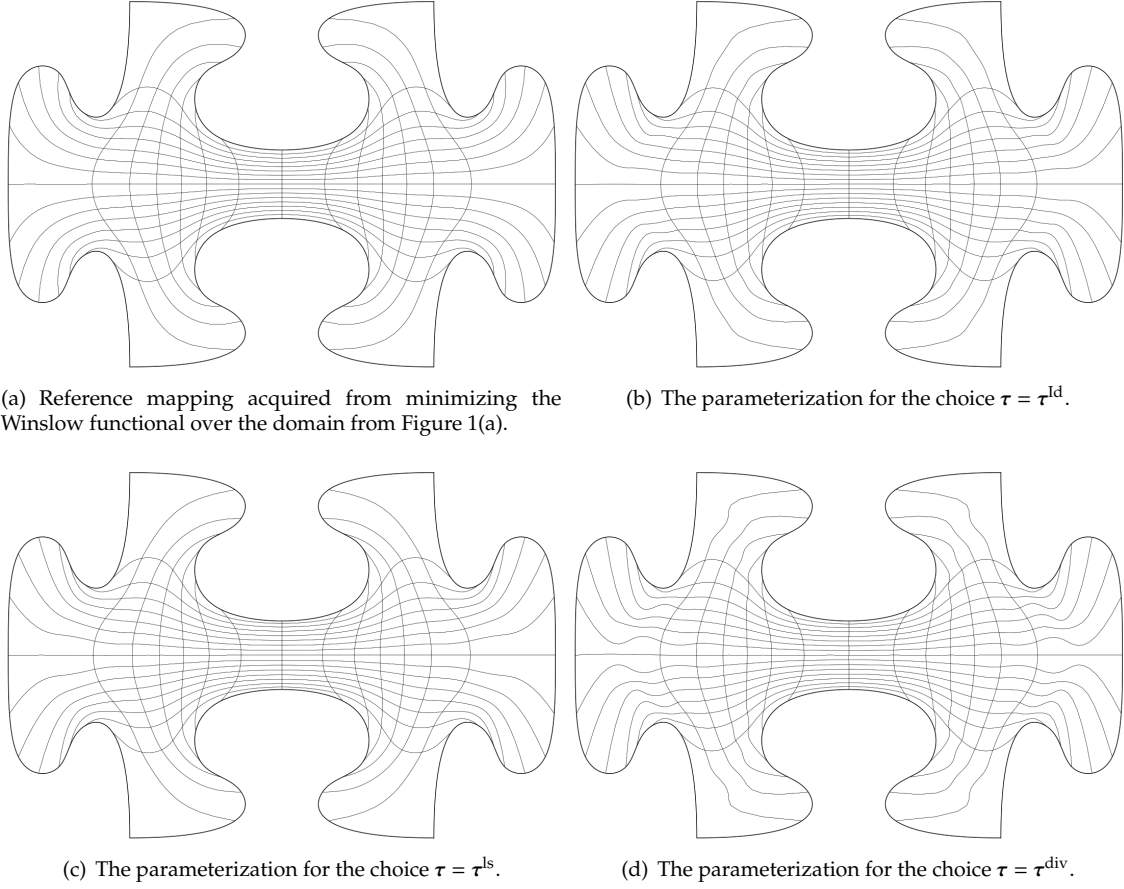


Figure 2: Parameterizations acquired using the various discretization techniques.

However, the figure shows noticeable differences in the parametric properties between the various methods, in particular in the protruded parts and in particular in Figure 2(d). Upon uniform refinement, the differences become less pronounced, suggesting that all schemes are consistent. Table 1 shows the outcomes of substituting the various parameterizations into (37). Not surprisingly, the choice $\tau = \tau^{div}$ fares the worst while the table suggests that $\tau = \tau^{ld}$ is the best choice. Upon refinement, the $\tau = \tau^{ld}$ and $\tau = \tau^{ls}$ parameterizations become virtually indistinguishable from the global minimizer over the coarse space, which is also reflected in table 1.

As documented in the literature [9], all parameterizations suffer from the well-known pathologies of inversely harmonic maps, such as the tendency to yield large elements within protruded parts. Fortunately, in a THB-setting this can be easily compensated for by performing local refinement in the affected regions. Mitigating the impact of these pathologies will be the topic of Section 4.

2.6. The Role of PDE-Based Parameterization in Shape Optimization Applications

The monolithic approach toward geometry parameterization and the numerical treatment of PDE-problems posed over the geometry, made possible by the isoparametric principle, has a number of interesting applications to IGA-based shape optimization (SO) problems. Let the SO-problem be posed over a design space

$$\mathbf{f}_l(\alpha) \leq \alpha \leq \mathbf{f}_u(\alpha) \quad (39)$$

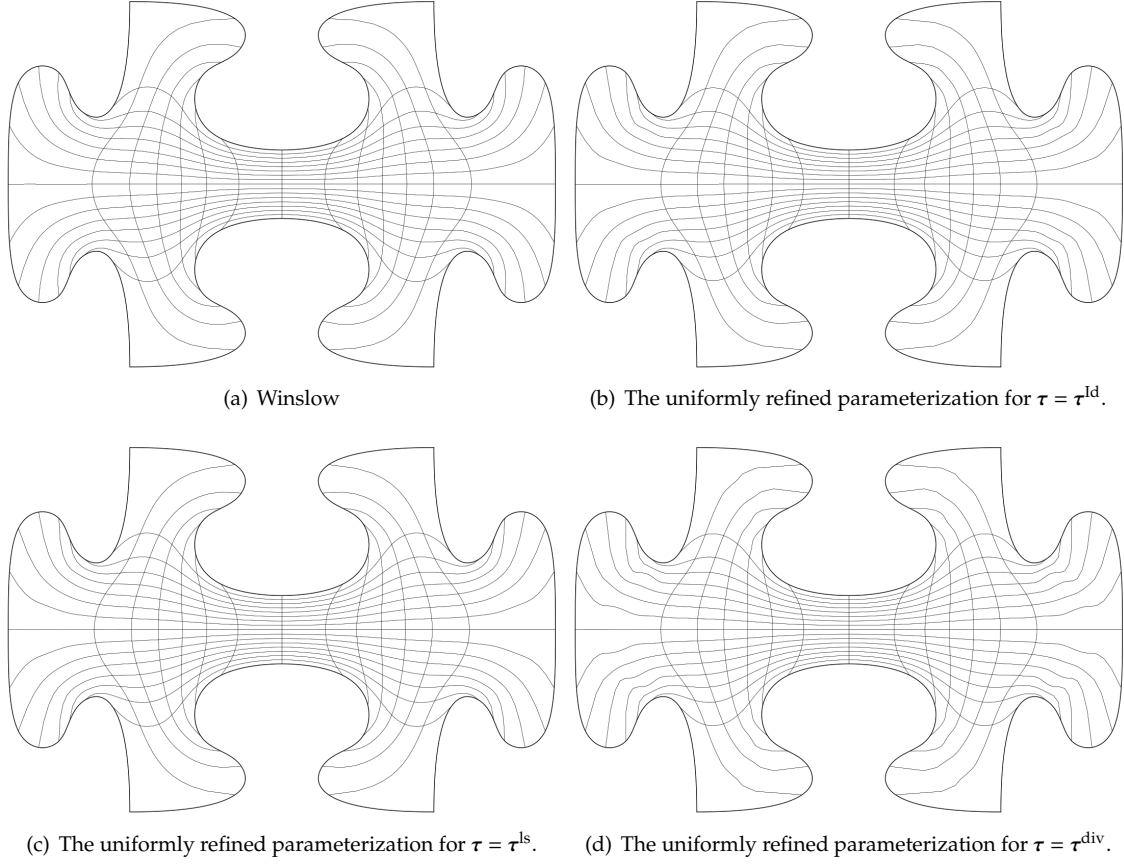


Figure 3: Parameterizations acquired using the various discretization techniques over the refined domain.

with the n -dimensional vector of design variables $\alpha = (\alpha_1, \dots, \alpha_n)^T$ and let

$$\mathcal{V}^{\alpha, f} = \{v \in \mathcal{V} \mid v = f(\mathbf{x}^\alpha) \text{ on } \partial\Omega_D^\alpha\}, \quad (40)$$

for some $\partial\Omega_D^\alpha \subseteq \partial\Omega^\alpha$ and an appropriately-chosen test space \mathcal{V} .
An SO-problem typically takes the form

$$\begin{aligned} J(u^\alpha, \mathbf{x}^\alpha) &\rightarrow \min_{\alpha} \\ \text{s.t. } \mathbf{f}_l(\alpha) &\leq \alpha \leq \mathbf{f}_u(\alpha), \end{aligned} \quad (41)$$

with $u^\alpha \equiv u(\mathbf{x}^\alpha)$ the solution of

$$\text{find } u(\mathbf{x}^\alpha) \in \mathcal{V}^{\alpha, u_D} \quad \text{s.t.} \quad \mathbf{R}(u(\mathbf{x}^\alpha), \phi, \mathbf{x}^\alpha) = \mathbf{0}, \quad \forall \phi \in \mathcal{V}^{\alpha, 0}, \quad (42)$$

for some differentiable form $\mathbf{R}(\cdot, \cdot, \cdot)$ and a function $u_D(\mathbf{x})$ that parameterizes the Dirichlet data for u . Here, $\mathbf{x}^\alpha \equiv \mathbf{x}(\alpha)$ parameterizes the geometry Ω^α as a function of the design variables and u denotes some solution field (temperature, pressure, ...). The dependency of the objective function $J(\cdot, \cdot)$ on \mathbf{x}^α results from it typically being an integral quantity over Ω^α and / or $\partial\Omega^\alpha$.

Typically, \mathbf{x}^α is computed from a closed-form expression [22], facilitating differentiation of $J(\cdot, \cdot)$ but limiting the optimization to relatively simple shapes. As the domain of the last argument of $\mathbf{R}(\cdot, \cdot, \cdot)$ is the set of all

bijjective \mathbf{x} with appropriate regularity, for given α , we may choose \mathbf{x}^α as the solution of

$$\text{find } \mathbf{x}^\alpha(\alpha) \in \mathcal{V}^{\alpha, \mathbf{x}_D} \quad \text{s.t.} \quad F(\mathbf{x}^\alpha(\alpha), \sigma) = 0, \quad \forall \sigma \in \mathcal{V}^{\alpha, 0}, \quad (43)$$

with $F(\mathbf{x}, \sigma)$ as defined in (23) and

$$\mathcal{V}^{\alpha, \mathbf{f}} = \{\mathbf{v} \in \mathcal{V}^2 \mid \mathbf{v} = \mathbf{f}(\alpha) \text{ on } \partial\hat{\Omega}\}. \quad (44)$$

Here $\mathbf{x}_D(\alpha) : \partial\hat{\Omega} \rightarrow \mathbb{R}^2$ parameterizes $\partial\Omega^\alpha$ for given α .

Following the optimize then discretize approach, we approximate the tuple $(u^\alpha, \mathbf{x}^\alpha)$ by $(u_h^\alpha, \mathbf{x}_h^\alpha)$, which follows from replacing \mathcal{V} by a finite-dimensional $\mathcal{V}_h \subset \mathcal{V}$ in (40) and (44). Furthermore, we replace (u_D, \mathbf{x}_D) by proper collocations (u_D^h, \mathbf{x}_D^h) that are compatible with \mathcal{V}_h . For given α , we approximate

$$J(u^\alpha, \mathbf{x}^\alpha) \simeq J(u_h^\alpha, \mathbf{x}_h^\alpha) \quad (45)$$

and

$$\frac{dJ}{d\alpha} \simeq \left(\frac{\partial J}{\partial u_h^\alpha} \frac{\partial u_h^\alpha}{\partial \alpha} + \frac{\partial J}{\partial \mathbf{x}_h^\alpha} \frac{\partial \mathbf{x}_h^\alpha}{\partial \alpha} \right). \quad (46)$$

The implicit function theorem admits deriving a symbolic expression for $\partial_\alpha \mathbf{x}_h^\alpha$ from the discretized counterpart of (43), allowing for gradient-based shape optimization on a wider variety of domains, without the need to resort to algorithmic differentiation [23]. Thanks to the optimize then discretize approach, the basis \mathcal{V}_h may be chosen differently in every iteration. We choose \mathcal{V}_h such that:

- The boundary $\partial\Omega_h^\alpha$ parameterized by $\mathbf{x}_D^h(\alpha)|_{\partial\hat{\Omega}}$ approximates $\partial\Omega^\alpha$ well;
- \mathbf{x}_h^α is analysis suitable (i.e., bijective and preferably of high numerical quality);
- u_h^α is a good approximation of u^α .

Being able to satisfy the preceding requirements is one of the main motivations to combine PDE-based parameterization techniques with THB-splines, thanks to local refinement. Hence, choosing an appropriate basis \mathcal{V}_h will be one of the main topics of this work.

The gradient from (46) can be efficiently computed using an adjoint approach, for details see [24].

3. A Basic Scheme Based on a Posteriori Refinement

As stated in subsection 2.6, one of the main challenge of PDE-based parameterization lies in selecting an appropriate finite-dimensional spline basis \mathcal{V}_h . For this, we employ the technique of *Dual Weighted Residual*, which will be the topic of Subsection. 3.1.

3.1. Dual Weighted Residual

Dual weighted residual, as introduced by Rannacher et al. [4], is an a posteriori refinement strategy that is based on duality considerations. Consider a semi-linear differential form $A(u, \phi)$. We consider the problem

$$\text{find } u \in \mathcal{V}^0 \quad \text{s.t.} \quad A(u, \phi) = f(\phi), \quad \forall \phi \in \mathcal{V}^0, \quad (47)$$

for some linear functional $f(\cdot)$ and a suitably-chosen Hilbert space \mathcal{V} . We seek an approximate solution $u_h \in \mathcal{V}_h^0$ with $\mathcal{V}_h \subset \mathcal{V}$ by solving a discretized counterpart of (47)

$$\text{find } u_h \in \mathcal{V}_h^0 \quad \text{s.t.} \quad A(u_h, \phi_h) = f(\phi_h), \quad \forall \phi_h \in \mathcal{V}_h^0. \quad (48)$$

Let $L(u)$ be such that

$$\Delta L(u_h) \equiv L(u) - L(u_h) \quad (49)$$

is a quantity of interest (such as Δu in Poisson problems). Furthermore, let

$$\rho(u, \psi) = f(\psi) - A(u, \psi). \quad (50)$$

If z is the solution of

$$\text{find } z \in \mathcal{V}^0 \quad \text{s.t.} \quad A'(u, \phi, z) = L'(u, \phi), \quad \forall \phi \in \mathcal{V}^0, \quad (51)$$

we have

$$\Delta L(u_h) = \rho(u_h, z - \psi_h) + R_h(e), \quad (52)$$

for arbitrary $\psi_h \in \mathcal{V}_h^0$ and some R_h that is quadratic in $e \equiv u - u_h$. In practice, we neglect R_h and approximate z by the solution of the discrete adjoint equation

$$\text{find } z_h \in \bar{\mathcal{V}}_h^0 \quad \text{s.t.} \quad A'(u_h, \sigma_h, z_h) = L'(u_h, \sigma_h), \quad \forall \sigma_h \in \bar{\mathcal{V}}_h^0, \quad (53)$$

for some adjoint basis $\bar{\mathcal{V}}_h \subset \mathcal{V}$, such that

$$\Delta L(u_h) \simeq \rho(u_h, z_h - \psi_h) = \sum_{w_i \in \mathcal{V}_h} \rho(u_h, w_i(z_h - \psi_h)) \equiv \sum_i \mathbf{r}_i(\mathbf{x}_h), \quad (54)$$

thanks to semi-linearity of $A(\cdot, \cdot)$ and the partition of unity property associated with \mathcal{V}_h .

The motivation to use an adjoint basis that differs from \mathcal{V}_h is the fact that substituting any $z_h \in \mathcal{V}_h^0$ in (54) results in $\Delta L(u_h) = 0$, making it a lousy approximation due to Galerkin orthogonality.

The appeal of using (54) is that a scalar quantity of interest $\Delta L(u_h)$ is transformed into an integral quantity over $\bar{\Omega}$, which in turn is decomposed into the basis function wise contributions $\mathbf{r}_i(\mathbf{x}_h)$. The vector $\mathbf{r}(\mathbf{x}_h)$ may then be utilized in selecting basis functions for goal-oriented refinement (see Section 3.4).

Remark. If u_h is a very inaccurate approximation of u , the discrete adjoint solution z_h will be inaccurate regardless of the choice of $\bar{\mathcal{V}}_h$. Heuristically, we have rarely encountered this situation in the examples considered in this work. In case refinement is ineffective, the procedure should be restarted with a uniformly refined initial basis.

3.2. Applications to PDE-Based Parameterization

We now apply the methodology from subsection 3.1 to the PDE-based parameterization problem (22). Let \mathbf{x}_D be the canonical extension of the Dirichlet data from (22). With $\mathbf{x}_h = \mathbf{x}_D + \mathbf{x}_0$, we may write (22) in the equivalent form

$$\text{find } \mathbf{x}_0 \in \mathcal{V}_h^0 \quad \text{s.t.} \quad F(\mathbf{x}_D + \mathbf{x}_0, \sigma_h) = 0, \quad \forall \sigma_h \in \mathcal{V}_h^0. \quad (55)$$

In the formalism of (48), we hence have $A(\mathbf{x}, \sigma) = F(\mathbf{x}_D + \mathbf{x}, \sigma)$ and $f(\sigma) = 0$. Alternatively, we may absorb the dependence on \mathbf{x}_D in $f(\cdot)$.

We would like to design scalar cost functions ($L(u)$ in (49)) to aid us in refining an a priori chosen basis \mathcal{V}_h such that after recomputing the solution over the refined space $\mathcal{V}_h^R \supset \mathcal{V}_h$,

1. \mathbf{x}_h^R is bijective;
2. \mathbf{x}_h^R approximates \mathbf{x} well.

In a discrete setting, we may relax the condition that \mathbf{x}_h^R be bijective by the condition that \mathbf{x}_h^R has a positive Jacobian determinant in all quadrature points $\Xi = \{\xi_1^q, \dots, \xi_M^q\}$.

As such, let \mathbf{x}_h be the solution of (55) over the space \mathcal{V}_h and let

$$\Xi_- = \{\xi_i^Q \in \Xi \mid \det J(\mathbf{x}_h) < 0 \text{ in } \xi_i^Q\}. \quad (56)$$

To address (potential) lack of bijectivity, we propose the following goal-oriented cost function:

$$L_\Xi(\mathbf{x}) = \sum_{\xi_i^Q \in \Xi_-} \det J(\mathbf{x})(\xi_i^Q), \quad (57)$$

such that

$$\Delta L_\Xi(\mathbf{x}_h) = \underbrace{L_\Xi(\mathbf{x})}_{\geq 0} - \underbrace{L_\Xi(\mathbf{x}_h)}_{\leq 0} \geq 0, \quad (58)$$

with equality if and only if $\Xi_- = \emptyset$. Here, the inequality $L(\mathbf{x}) \geq 0$ follows from the Radó-Kneser-Choquet theorem (see Section 1) while $L(\mathbf{x}_h) \leq 0$ follows from (56). According to (54), we may approximate

$$\Delta L_\Xi(\mathbf{x}_h) \simeq -F(\mathbf{x}_h, \mathbf{z}_h - \boldsymbol{\psi}_h) = \sum_{w_i \in \mathcal{V}_h} -F(\mathbf{x}_h, w_i(\mathbf{z}_h - \boldsymbol{\psi}_h)) \equiv \sum_i \mathbf{r}_i(\mathbf{x}_h). \quad (59)$$

Typically, we choose $\boldsymbol{\psi}_h$ as the $L_2(\hat{\Omega}, \mathbb{R}^2)$ -projection of \mathbf{z}_h onto \mathcal{V}_h^0 .

Remark. Even though subtracting a nonzero $\boldsymbol{\psi}_h \in \mathcal{V}_h^0$ does not alter the outcome on the right hand side of (59), it does influence its decomposition into the basis function wise contributions $\mathbf{r}_i(\mathbf{x}_h)$.

Strategies for refinement based on the basis function wise contributions $\mathbf{r}_i(\mathbf{x}_h)$ will be the topic of Section 3.4. After refinement of \mathcal{V}_h , we recompute the mapping from the enriched basis \mathcal{V}_h^R and if necessary repeat above steps until discrete bijectivity (over Ξ) has been achieved.

Remark. For better performance, we always use the prolonged coarse grid solution as an initial guess for recomputing the mapping under the refined basis.

Upon completion, we may choose to settle for the (possibly inaccurate but analysis-suitable) resulting mapping \mathbf{x}_h^R , or we may choose to further-improve its accuracy. As solving (43) is equivalent to minimizing (37), by choosing $-L_W(\mathbf{x})$ as cost function, we acquire the quantity of interest

$$\Delta L_W(\mathbf{x}_h) = -L_W(\mathbf{x}) + L_W(\mathbf{x}_h) \geq 0, \quad (60)$$

with equality if and only if $\|\mathbf{x} - \mathbf{x}_h\|_{H^1(\hat{\Omega})} = 0$. As such, (60) may serve as a measure for the distance of \mathbf{x}_h to \mathbf{x} . As before, we approximate (60) by substituting the discrete adjoint solution \mathbf{z}_h in (54) and base refinement criteria on the basis function wise contributions to (60). The steps of refinement, recompute and adjoint estimation may be repeated until the estimate $|\Delta L_W(\mathbf{x}_h)| \simeq |-F(\mathbf{x}_h, \mathbf{z}_h - \boldsymbol{\psi}_h)|$ is deemed sufficiently small. Above methodology is compatible with the direct approach from Section 2.4. A typical work flow consists of computing a bijection \mathbf{x}_h under the cost function (57) in combination with an indirect approach and continuing to improve parametric quality using (60) in combination with direct minimization once convergence of (38) is achieved with \mathbf{x}_h .

3.3. Choice of Adjoint Basis

Problem (53) requires choosing a suitable dual basis $\mathcal{V}^2 \supset \bar{\mathcal{V}}_h \neq \mathcal{V}_h$, which typically results from uniformly refining \mathcal{V}_h (in either h or p), leading to a ~ 4 -fold increase in the number of DOFs associated with the (linear) discrete adjoint equation. In a THB-setting, we have the luxury of choosing $\bar{\mathcal{V}}_h$ reminiscent of the role of K -refinement [25] in a structured spline setting. Let (p, α) be the degree and regularity of \mathcal{V}_h (which we assume to be equal in both directions for convenience) and let \mathcal{T} denote the corresponding decomposition of

$\hat{\Omega}$ into elements. We define $\bar{\mathcal{V}}_K(\mathcal{V}_h)$ as the richest (cardinality-wise) THB basis of degree $p + 1$ and regularity $\alpha + 1$ that is compatible with the elements in \mathcal{T} . Typically, we have $|\bar{\mathcal{V}}_K(\mathcal{V}_h)| \approx |\mathcal{V}_h|$. While taking $\bar{\mathcal{V}}_h = \bar{\mathcal{V}}_{h/2}^2$ yields more accurate adjoint solutions \mathbf{z}_h , we have found the choice $\bar{\mathcal{V}}_h = \bar{\mathcal{V}}_K^2(\mathcal{V}_h)$, to be sufficient for refinement based on both (56) and (60). As such, solving the discrete adjoint equation becomes a cheap operation.

3.4. Refinement Strategies

The decomposition into basis function wise contributions $\mathbf{r}_i(\mathbf{x}_h)$ introduced in (54) is particularly useful in a THB-setting since elementwise refinement may not change the cardinality of the underlying THB spline space. In the following, we present several strategies for using $\mathbf{r}(\mathbf{x}_h)$ to mark basis functions $w_i \in \mathcal{V}_h$ for refinement. We define the vectors \mathbf{w} and $\tilde{\mathbf{r}}$ with

$$\mathbf{w}_i = \int_{\hat{\Omega}} w_i dS \quad \text{and} \quad \tilde{\mathbf{r}}_i = \frac{\mathbf{r}_i}{\mathbf{w}_i}. \quad (61)$$

Furthermore, we let $\tilde{\mathbf{r}}_{\max} = \max_i |\tilde{\mathbf{r}}_i|$ and $\mathcal{I} = \{1, \dots, |\mathcal{V}_h|\}$. Inspired by [26], we define

$$\mathcal{I}_{\max}^\alpha = \{i \in \mathcal{I} \mid |\tilde{\mathbf{r}}_i| \geq \alpha \tilde{\mathbf{r}}_{\max}\} \quad (62)$$

as the index-set of absolutely weighted contributions that exceed the value $\alpha \tilde{\mathbf{r}}_{\max}$, for some $\alpha \in [0, 1]$. The $i \in \mathcal{I}_{\max}^\alpha$ then constitute the indices corresponding to basis functions whose supporting elements $\mathcal{E}^k \in \mathcal{T}$, from the k -th level in the element hierarchy, are replaced by finer counterparts \mathcal{E}^{k+1} from the $(k + 1)$ -th level. Since both (57) and (60) are strictly positive quantities of interest, disregarding negative contributions in (61) is a plausible strategy, too. Heuristically, this strategy mildly reduces the total number of required DOFs until bijectivity is achieved. However, this comes at the expense of a larger number of the required a posteriori refinements, which are limited to typically no more than 3 – 4 using (62).

3.5. Results

To demonstrate the appeal of local refinement made possible by THB splines, in the following, we present parameterizations for the U.S. state of Indiana, the German province of North Rhine-Westphalia and the country of Austria, all of which have complicated boundaries but relatively simple interior. The initial basis \mathcal{V}_h results from refining an initial grid comprised of 7×7 elements by the boundaries until the boundary contours are approximated sufficiently well. In all cases, \mathcal{V}_h is a bicubic hierarchical basis and we take $\bar{\mathcal{V}}_h = \bar{\mathcal{V}}_K^2(\mathcal{V}_h)$ (see Section 3.3) and base refinement on (62) with $\alpha = 0.2$.

Figures (4) to (5) clearly demonstrate the DOF savings made possible by local refinement. Not surprisingly, refinement especially affects the protruded and concave areas close to the boundaries.

At every refinement level, parameterizations were computed using the Newton approach from Section 2.1. All parameterizations were post-processed with the direct approach from Section 2.4 once bijectivity had been achieved.

The iterative solver typically converges after 4 – 5 nonlinear iterations on the coarsest level plus another 2 – 3 iterations per a posteriori refinement. Since the solutions of direct and indirect formulations are very close, convergence is reached after just a few iterations.

4. Domain Optimization

As demonstrated in Section 3.5, the approach from Section 3 can handle challenging geometries. However, it lacks the flexibility of precisely controlling the parametric properties of the outcome, which may lead to undesirable features, such as large elements (see Figures 2 and 3). As such, in the following we present a framework that allows for more flexibility, where we pay particular attention to mitigating the aforementioned pathologies associated with inversely harmonic maps.

Instead of taking the domain static, we now define it through a parameterization $\mathbf{s} : \hat{\Omega} \rightarrow \hat{\Omega}$. For convenience,

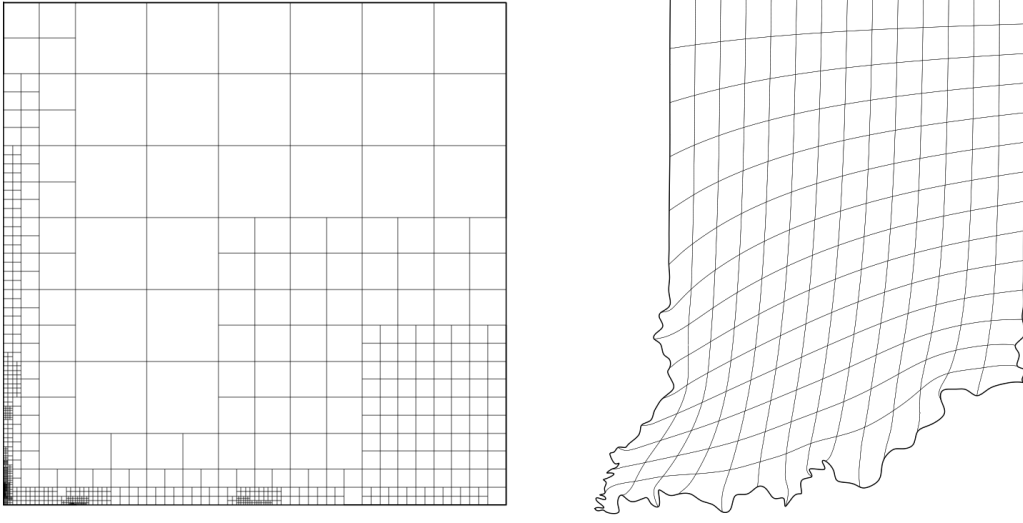


Figure 4: The domain with canonical bicubic basis of 2338 DOFs (left) and the THB-spline parameterization of the U.S. state of Indiana (right).

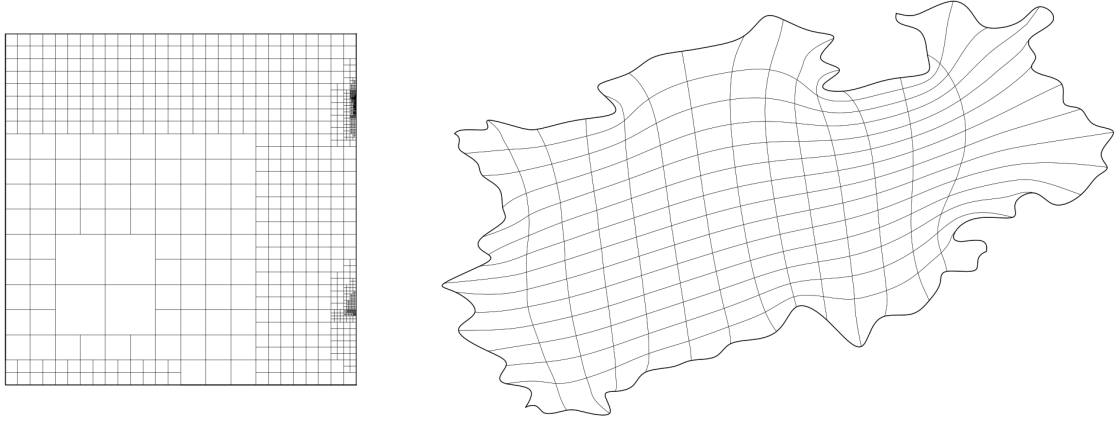


Figure 5: The domain with bicubic basis of 2676 DOFs (left) and the THB-spline parameterization of the German province of North Rhine-Westphalia (right).

we assume that the boundary correspondence $\mathbf{s}|_{\partial\hat{\Omega}} : \partial\hat{\Omega} \rightarrow \partial\hat{\Omega}$ is the identity. Suppose that $\mathbf{x}^* : \hat{\Omega} \rightarrow \Omega$ solves the equation

$$\Delta_{\mathbf{x}} \xi = 0, \quad \text{s.t.} \quad \mathbf{x}|_{\partial\hat{\Omega}} = \mathbf{x}_D(\xi), \quad (63)$$

for \mathbf{x} . Then, if $\mathbf{x}(\xi)$ is the solution of

$$\Delta_{\mathbf{x}} \mathbf{s}(\xi) = 0, \quad \text{s.t.} \quad \mathbf{x}|_{\partial\hat{\Omega}} = \mathbf{x}_D(\mathbf{s}(\xi)), \quad (64)$$

it clearly satisfies $\mathbf{x} = \mathbf{x}^* \circ \mathbf{s}$, thanks to the fact that $\mathbf{x}_D \circ \mathbf{s} = \mathbf{x}_D$, on $\partial\hat{\Omega}$ (i.e., the boundary condition does not change upon pullback). As such, we may approximate compositions $\mathbf{x}^* \circ \mathbf{s}$ by solving the discretized counterpart of (64).

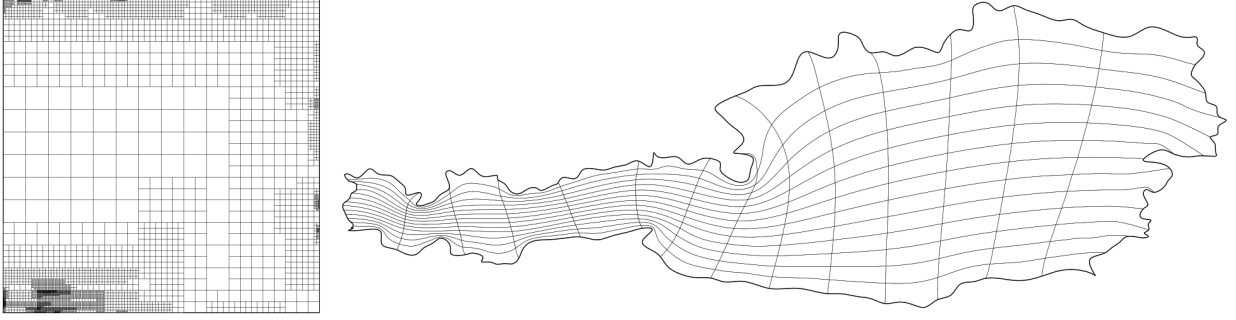


Figure 6: The domain with bicubic basis comprised of 9640 DOFs (left) and the THB-spline parameterization of Austria (right).

Introducing the set of vectors

$$\mathbf{p}^{ij}(\mathbf{s}) = -T^{-1} \frac{\partial^2 \mathbf{s}}{\partial \xi_i \partial \xi_j}, \quad \text{with } T = \partial_\xi \mathbf{s}, \quad (65)$$

it can be shown that with $\mathbf{s} = \mathbf{s}(\xi)$, (64) can be reformulated as [19]

$$A(\mathbf{x}) : \left(H(\mathbf{x}_i) + P^1(\mathbf{s}) \frac{\partial \mathbf{x}_i}{\partial \xi} + P^2(\mathbf{s}) \frac{\partial \mathbf{x}_i}{\partial \eta} \right) = 0 \quad i \in \{1, 2\}, \quad \text{s.t. } \mathbf{x}|_{\partial \hat{\Omega}} = \mathbf{x}_D, \quad (66)$$

where the matrices P^1 and P^2 satisfy

$$P_{ij}^k(\mathbf{s}) = \mathbf{p}_k^{ij}(\mathbf{s}), \quad k \in \{1, 2\}. \quad (67)$$

Therefore, we introduce

$$F_\tau(\mathbf{x}, \sigma, \mathbf{s}) = \int_{\hat{\Omega}} \tau(\sigma, \mathbf{x})_i A(\mathbf{x}) : \underbrace{\left(H(\mathbf{x}_i) + P^1(\mathbf{s}) \frac{\partial \mathbf{x}_i}{\partial \xi} + P^2(\mathbf{s}) \frac{\partial \mathbf{x}_i}{\partial \eta} \right) \det T(\mathbf{s})}_{\tilde{H}(\mathbf{x}_i, \mathbf{s})} dS, \quad (68)$$

and for given $\mathbf{s}(\xi)$, we solve

$$\text{find } \mathbf{x}_h \in \mathcal{V}_h^{\mathbf{x}_D} \quad \text{s.t.} \quad F_\tau(\mathbf{x}_h, \sigma_h, \mathbf{s}) = 0 \quad \forall \sigma_h \in \mathcal{V}_h^0, \quad (69)$$

in order to approximate $\mathbf{x}^* \circ \mathbf{s}$. Unless stated otherwise, we utilize the Newton approach from Section 2.1 with $\tau(\sigma, \mathbf{x}) = \sigma$. We can apply the Picard approach from Section 2.3 by replacing $H(\mathbf{x}_i) \rightarrow \tilde{H}(\mathbf{x}_i, \mathbf{s})$ in equation (33). In the following, we present several strategies for choosing \mathbf{s} to improve the parametric properties of the composite mapping.

Remark. Including the measure $\det T$ in (22) removes the $(\det T)^{-1}$ -dependence in the matrices P^k (see (67)).

4.1. Exploiting the Maximum Principle

Clearly, for well-posedness of (69), $\mathbf{s} : \hat{\Omega} \rightarrow \hat{\Omega}$ should not fold. As the control mapping maps into a convex domain, we may exploit the fact that if it is comprised of harmonic functions, it is necessarily a bijection. Thus, let $\mathbf{s} = (\mathbf{s}_1, \mathbf{s}_2)^T$ be such that

$$\nabla_\xi \cdot (D_i \partial_\xi \mathbf{s}_i) = 0 \quad i \in \{1, 2\}, \quad \text{in } \hat{\Omega}, \quad \text{s.t. } \mathbf{s}(\xi) = \xi \text{ on } \partial \hat{\Omega}, \quad (70)$$

where the $D_i : \hat{\Omega} \rightarrow \mathbb{R}^{2 \times 2}$ are both SPD diffusivity tensors. In the following, we assume that an accurate approximation \mathbf{x}_h^* of \mathbf{x}^* has been computed using the methodology from Section 3. In order to mitigate the impact of the well-known pathologies of inversely harmonic maps (see Section 2), we may select the D_i in (70) such that the value of

$$L_{\text{Area}}(\mathbf{x}_h) = \int_{\hat{\Omega}} \det J(\mathbf{x}_h)^2 dS \quad (71)$$

is expected to decrease with respect to \mathbf{x}^* (see (12)). Note that

$$(\det J(\mathbf{x}^* \circ \mathbf{s}))^2 \simeq (\det \partial_s \mathbf{x}_h^*)^2 \det J(\mathbf{s})^2 = (\det \partial_s \mathbf{x}_h^*)^2 (g_{11}g_{22} - g_{12}^2)_{\xi \rightarrow \mathbf{s}} \leq \frac{1}{2} (\det \partial_s \mathbf{x}_h^*)^2 (g_{11} + g_{22})_{\xi \rightarrow \mathbf{s}}^2, \quad (72)$$

where the subscript $\xi \rightarrow \mathbf{s}$ indicates that the g_{ij} between brackets refer to the metric between ξ and $\mathbf{s}(\xi)$. Given that $\mathbf{s}(\xi) = \xi$ initially, (72) suggests a convex optimization problem of the form

$$L_{\text{PoissonArea}}(\mathbf{s}, k) \rightarrow \min_{\mathbf{s} \in \mathcal{V}_h^2}, \quad \text{s.t.} \quad \mathbf{s}(\xi) = \xi \text{ on } \partial \hat{\Omega}, \quad (73)$$

where

$$L_{\text{PoissonArea}}(\mathbf{s}, k) = \int_{\hat{\Omega}} (\det \partial_{\xi} \mathbf{x}_h^*)^k (\|\partial_{\xi} \mathbf{s}_1\|^2 + \|\partial_{\xi} \mathbf{s}_2\|^2) dS, \quad (74)$$

for recomputing $\mathbf{s}(\xi)$. As such, we are solving the discretized equations corresponding to (70) with

$$D_1 = D_2 = (\det \partial_{\xi} \mathbf{x}_h^*)^k \mathcal{I}^{2 \times 2}. \quad (75)$$

Even though the exact solution of (70) does not fold, the discretized counterpart may fold due to extreme diffusive anisotropy. This can be counteracted by reducing the value of k . Alternatively, (74) can be utilized for DWR-based a posteriori refinement to achieve bijectivity and accuracy of $\mathbf{s} : \hat{\Omega} \rightarrow \hat{\Omega}$.

Upon completion, we compute \mathbf{x}_h from the basis utilized for $\mathbf{s} : \hat{\Omega} \rightarrow \hat{\Omega}$, with a posteriori refinement if necessary.

k	0	0.5	1	1.5
$L_{\text{Area}}(\mathbf{x}_h) \times 10^{-2}$	3.291	2.077	1.439	1.299

Table 2: Evaluation of $L_{\text{Area}}(\mathbf{x}_h)$ for various values of k .

Figure 7 shows puzzle piece geometry parameterizations for various values of k , while Table 2 contains the outcomes of substituting into (71). Both clearly demonstrate that the methodology has the desired effect, with more drastic outcomes for larger values of k . Figure 8 shows the isolines of $\mathbf{s}(\xi)$ before and after reparameterization with $k = 1.5$. All parameterizations were computed with the reference basis corresponding to Figure 7(a). No a posteriori refinements were necessary.

Figure 9 shows parameterizations of the U.S. state of Indiana for $k = 0$ and $k = 1$. Contrary to Table 2, with $L_{\text{Area}}(\mathbf{x}_h) = 1.049 \times 10^2$ for $k = 0$ and $L_{\text{Area}}(\mathbf{x}_h) = 1.008 \times 10^2$ for $k = 1$, the effect is very mild. Restricting the integrals to $\eta < 1/7$, however, the difference becomes more pronounced with $L_{\text{Area}}(\mathbf{x}_h) = 17.167$ and $L_{\text{Area}}(\mathbf{x}_h) = 14.118$, respectively. Unsurprisingly from the shape of the geometry, the difference is most striking close to the lower boundary, which can also be seen in the figure. A posteriori refinement was necessary in Figure 9(b).

Heuristically, reparameterization based on the maximum principle proves to be one of the most robust and effective choices for a wide range of geometries while being computationally efficient. This is thanks to the fact that it addresses the known pathologies of inversely harmonic maps, while also yielding smooth solutions, which preserves smoothness of the composite mapping.

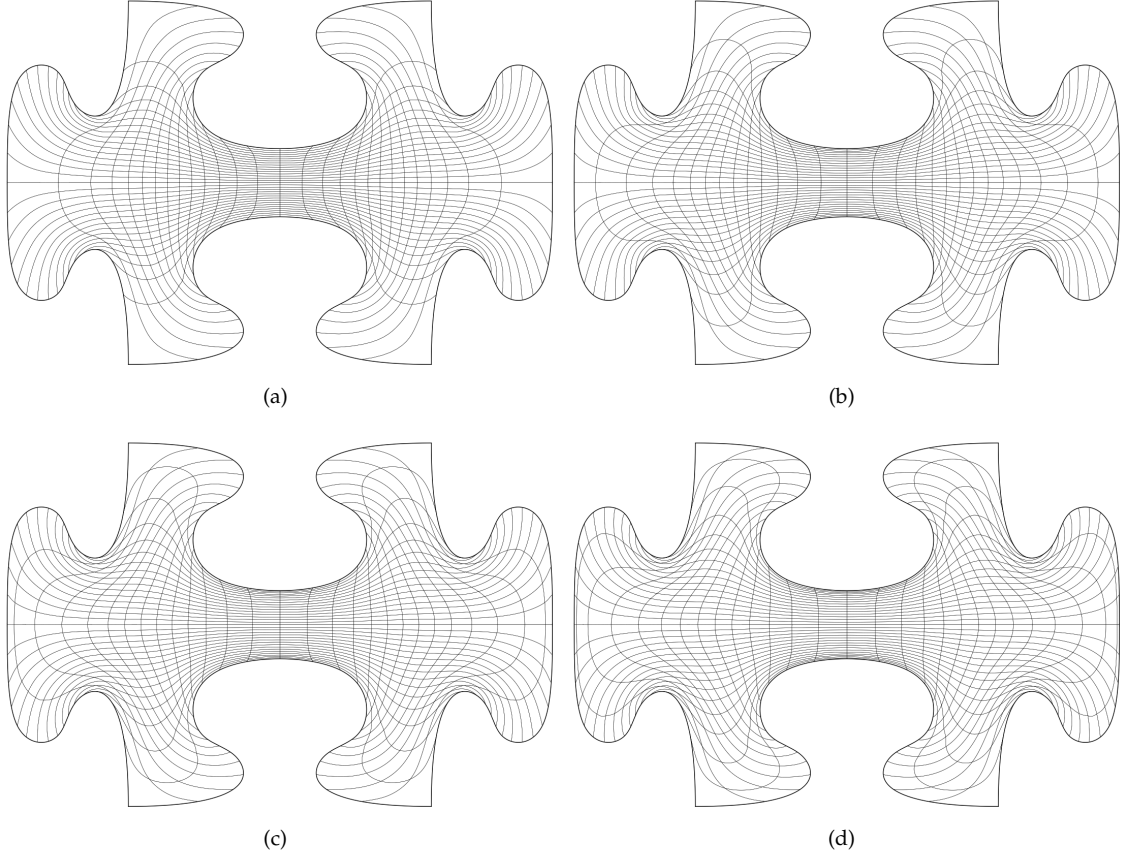


Figure 7: Several parameterizations of the puzzle piece with reparameterization based on (70) and (75) with the reference parameterization $k = 0$ (a), reparameterization with $k = 0.5$ (b), $k = 1$ (c) and $k = 1.5$ (d).

4.2. Constrained Domain Optimization

The concept of reparameterizing the domain in order to alter the parametric properties of the recomputed geometry parameterization can be further extended in a way more reminiscent of the well-known cost function minimization approach (see Section 1). Given an accurate approximation \mathbf{x}_h^* of \mathbf{x}^* (see Section 4.1), we define the metric $G_{\mathbf{s} \rightarrow \mathbf{x}} = \partial_{\mathbf{s}} \mathbf{x}^T \partial_{\mathbf{s}} \mathbf{x}$, which is initially given by $G_{\mathbf{s} \rightarrow \mathbf{x}} = \partial_{\xi} \mathbf{x}^{*T} \partial_{\xi} \mathbf{x}^* \simeq \partial_{\xi} \mathbf{x}_h^{*T} \partial_{\xi} \mathbf{x}_h^*$. Hence, in order to optimize $\mathbf{x}_h(\xi)$, we optimize $\mathbf{s}(\xi)$ in the metric induced by $G_{\mathbf{s} \rightarrow \mathbf{x}}$. With

$$g_{ij}^{\mathbf{s}} = \left[\partial_{\xi} \mathbf{s}^T G_{\mathbf{s} \rightarrow \mathbf{x}} \partial_{\xi} \mathbf{s} \right]_{ij} \quad \text{and} \quad J_{ij}^{\mathbf{s}} = (\partial_{\xi} \mathbf{x}_h^* \partial_{\xi} \mathbf{s})_{ij}, \quad (76)$$

we define domain optimization cost functions $Q_i^{\mathbf{s}}(\mathbf{s})$ by replacing $g_{ij} \rightarrow g_{ij}^{\mathbf{s}}$ and $J_{ij} \rightarrow J_{ij}^{\mathbf{s}}$ in the Q_i introduced in equation (6) (see Section 1). We may nevertheless choose to add terms of the form $Q_i(\mathbf{s})$, which should then be regarded as regularization terms. Let $\mathcal{V}_h^{\square} = \{\mathbf{v} \in \mathcal{V}_h^2 \mid \mathbf{v} = \xi \text{ on } \partial \hat{\Omega}\}$. A domain optimization problem takes the form

$$\int_{\hat{\Omega}} Q(\mathbf{s}) dS \rightarrow \min_{\mathbf{s} \in \mathcal{V}_h^{\square}}, \quad \text{s.t.} \quad \mathbf{C}(\mathbf{s}) \geq \mathbf{0}, \quad (77)$$

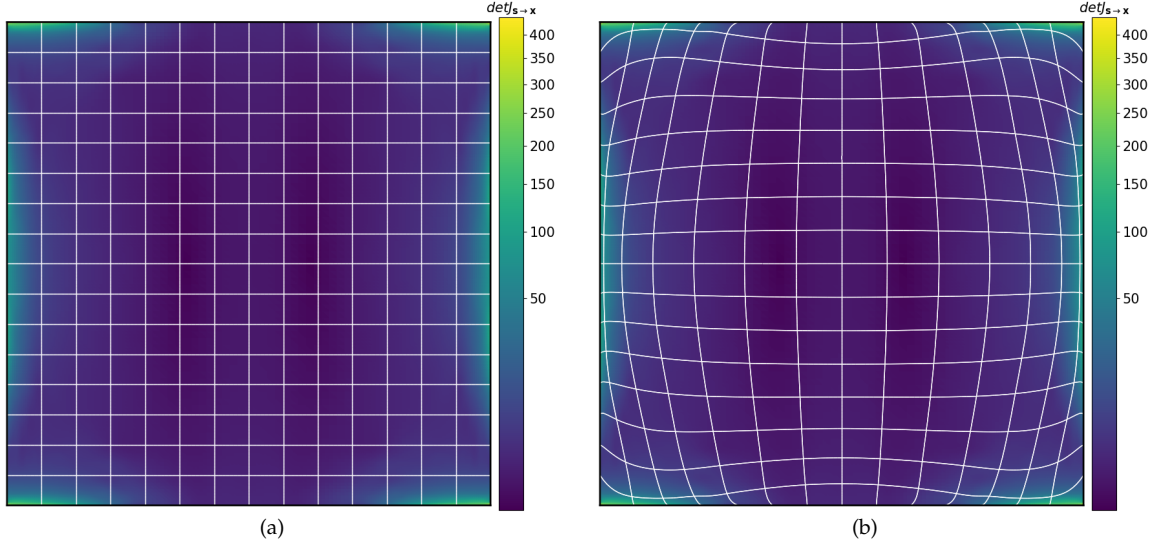


Figure 8: Plots showing the reference domain (a) and the reparameterized domain based on (70) and (75) with $k = 1.5$ (b). The figure clearly shows that the elements are contracted in the vicinity of large values of $\det \partial_s \mathbf{x}_h^*$.

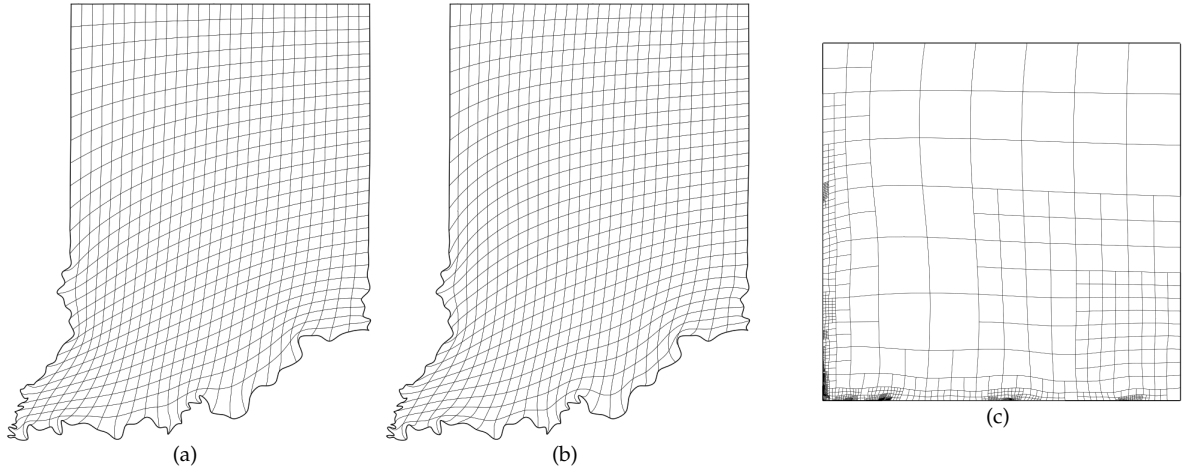


Figure 9: Parameterization of the U.S. state of Indiana with $k = 0$ (a), $k = 1$ (b) and the corresponding reparameterized domain (c).

with

$$Q(\mathbf{s}) = \sum_i \lambda_i^s Q_i^s(\mathbf{s}) + \sum_j \lambda_j Q_j(\mathbf{s}). \quad (78)$$

Here, the constraint $C(\mathbf{s}) \geq 0$ ensures that the minimizer of (77) does not fold. In the following, we list all choices of $C(\mathbf{s})$ that come to mind.

Given the element segmentation \mathcal{T} of $\hat{\Omega}$, by $\mathcal{V}^{p,\alpha}(\mathcal{T})$ we denote the canonical THB-basis with order p and regularity α that is compatible with \mathcal{T} . Note that $\alpha \leq p - 1$. Clearly, if \mathcal{V}_h has order p and regularity $\alpha \leq p - 1$, this implies that $\det \partial_\xi \mathbf{s} \in \mathcal{V}^{2p-1,\alpha-2}(\mathcal{T})$. As such, we also have $\det \partial_\xi \mathbf{s} \in \mathcal{V}^{2p-1,-1}(\mathcal{T})$. Hence, we can base the constraint on Bézier extraction, in which we impose that all weights of the projection of $\det \partial_\xi \mathbf{s}$ onto

$\mathcal{V}^{2p-1,-1}(\mathcal{T})$ be positive. Let $\hat{\mathbf{d}}$ be the corresponding vector of weights. We have

$$\hat{\mathbf{d}}(\mathbf{s}) = \hat{M}^{-1}\hat{\mathbf{f}}(\mathbf{s}) > \mathbf{0}, \quad \text{where} \quad \hat{\mathbf{f}}_i(\mathbf{s}) = \int_{\hat{\Omega}} \hat{\phi}_i \det \partial_{\xi} \mathbf{s} dS, \quad \text{with} \quad \hat{\phi}_i \in \mathcal{V}^{2p-1,-1}(\mathcal{T}) \quad \text{and} \quad \hat{M}_{i,j} = \int_{\hat{\Omega}} \hat{\phi}_i \hat{\phi}_j dS. \quad (79)$$

Note that \hat{M} is block-diagonal with $|\mathcal{T}|$ blocks of size $(2p, 2p)$. Hence, we computationally efficiently assemble \hat{M}^{-1} simply by computing the inverse of all separate blocks leading to a sparse block-diagonal matrix. As such, the computational costs of testing whether the condition $\hat{\mathbf{d}} \geq \mathbf{0}$ is fulfilled reduces to the assembly of $\hat{\mathbf{f}}$ along with one sparse matrix-vector multiplication. Assembly of the constraint gradient of $\hat{\mathbf{d}}(\mathbf{c}_I)$, where \mathbf{c}_I is a vector containing the inner control points of \mathbf{s} , requires the assembly of $\partial_{\mathbf{c}_I} \hat{\mathbf{d}}$ and a sparse matrix-matrix multiplication. The assembly is hence feasible. However, for large values of p this may lead to an infeasibly large number of constraints.

Inspired by [8], we formulate an alternative constraint by projecting $\det \partial_{\xi} \mathbf{s}$ onto the coarser THB-basis $\mathcal{V}^{2p,\alpha-2}(\mathcal{T})$. Similar to (79), this leads to a constraint of the form

$$\mathbf{d}(\mathbf{s}) = M^{-1}\mathbf{f}(\mathbf{s}) > \mathbf{0}, \quad \text{where} \quad \mathbf{f}_i(\mathbf{s}) = \int_{\hat{\Omega}} \phi_i \det \partial_{\xi} \mathbf{s} dS, \quad \text{with} \quad \phi_i \in \mathcal{V}^{2p-1,\alpha-2}(\mathcal{T}) \quad \text{and} \quad M_{i,j} = \int_{\hat{\Omega}} \phi_i \phi_j dS. \quad (80)$$

Increasing the values of p and α , unlike for (79), the length of \mathbf{d} in (80) increases only slowly (thanks to k -refinement). On the other hand, the matrix M is not block-diagonal and neither is it separable (unlike in a structured spline setting). As such, the assembly of the constraint gradient is prohibitively expensive. A remedy here is introducing the vector of slack variables $\mathbf{e} > \mathbf{0}$. The constraint from (80) can be reformulated as follows:

$$C_{\alpha}(\mathbf{s}, \mathbf{e}) = \mathbf{f}(\mathbf{s}) - M\mathbf{e} = \mathbf{0}, \quad \text{with} \quad \mathbf{e} > \mathbf{0}. \quad (81)$$

Hence, we avoid inversion with M at the expense of introducing an additional inequality constraint and changing the existing inequality constraint to an equality constraint. Note that we have:

$$\frac{\partial C_{\alpha}(\mathbf{s}, \mathbf{e})}{\partial(\mathbf{c}_I, \mathbf{e})} = \left[\frac{\partial \mathbf{f}}{\partial \mathbf{c}_I}, -M \right] \quad \text{and} \quad \frac{\partial \mathbf{e}}{\partial(\mathbf{c}_I, \mathbf{e})} = [0, I]. \quad (82)$$

Given a set of abscissae $\Xi = \{\xi_1^c, \dots, \xi_m^c\} \subset \mathbb{R}^2$, an alternative constraint $\mathbf{C}^{\Xi}(\mathbf{s})$ follows from requiring that

$$\epsilon_i^L \leq \det \partial_{\xi} \mathbf{s}(\xi_i^c) \leq \epsilon_i^U, \quad \forall i \in \{1, \dots, m\}, \quad (83)$$

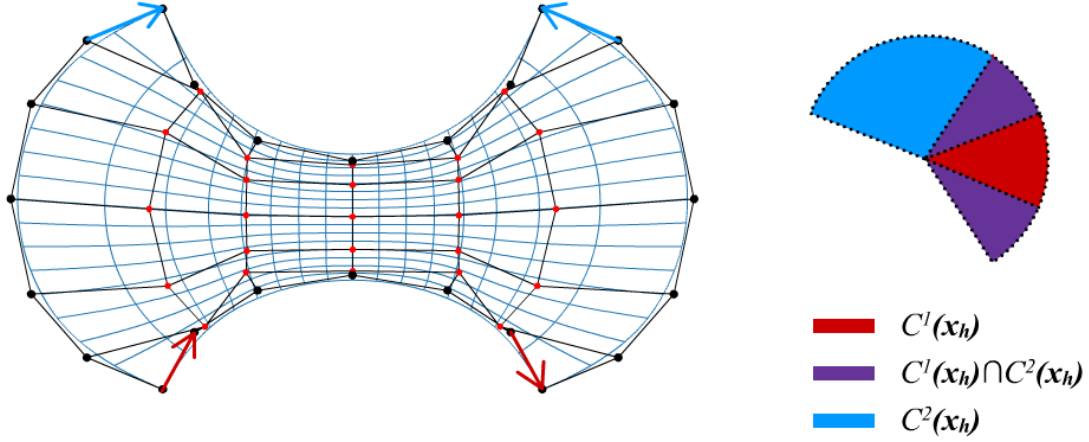
where $\mathbb{R}^m \ni \epsilon^{L,U} \geq 0$ are lower and upper thresholds. Note that (83) is nonlinear and nonconvex but not a sufficient condition for bijectivity of \mathbf{s} . However, it makes bijectivity likely for m sufficiently large.

Finally, assuming that \mathbf{s} is built from a structured basis $\mathcal{V}_h = \{N_1^{\square}, \dots, N_n^{\square}\} \times \{M_1^{\square}, \dots, M_m^{\square}\}$, we may alternatively utilize the linear constraint proposed in [10]. Typically, we take \mathcal{V}_h^{\square} as the cardinality-wise largest structured basis compatible with \mathcal{T} . Given

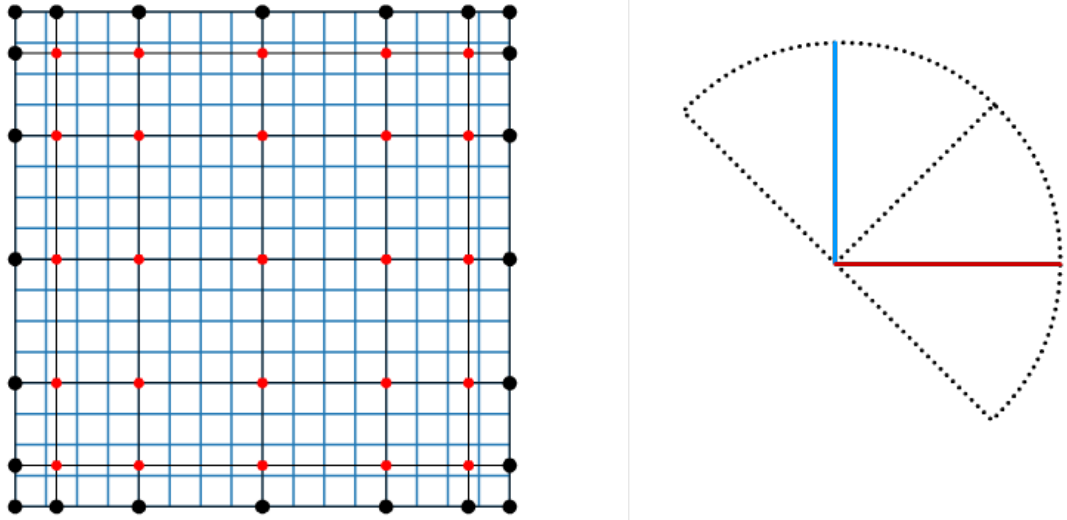
$$\mathbf{s}(\xi) = \sum_{i,j} \mathbf{c}_{i,j} N_i^{\square}(\xi) M_j^{\square}(\eta), \quad (84)$$

let the cones $C_1(\mathbf{s})$ and $C_2(\mathbf{s})$ be generated by the half rays $\mathbb{R}^+ \Delta_{i,j}^1$ and $\mathbb{R}^+ \Delta_{i,j}^2$ with

$$\Delta_{i,j}^1 = \mathbf{c}_{i+1,j} - \mathbf{c}_{i,j} \quad \text{and} \quad \Delta_{i,j}^2 = \mathbf{c}_{i,j+1} - \mathbf{c}_{i,j}, \quad (85)$$



(a) In this geometry, the constraint is violated despite the bijectivity of the mapping, demonstrating the restrictiveness of $\mathbf{C}^L(\mathbf{x}_h)$.



(b) In the case of the unparameterized domain, the linear constraint is much less restrictive.

Figure 10: Depiction of the bijectivity constraint \mathbf{C}^L . In (a), the constraint is violated since $C^1(\mathbf{x}_h) \cap C^2(\mathbf{x}_h) \neq \{\mathbf{0}\}$ despite the bijectivity of the mapping. In (b) we see that the unparameterized domain is located exactly in the center of the feasible region generated by the cones with $\theta(\Delta_{i,j}^1) \in (-\pi/4, \pi/4)$ and $\theta(\Delta_{i,j}^2) \in (\pi/4, 3\pi/4)$.

respectively. The constraint is based on the observation that if $C_1(\mathbf{s})$ and $C_2(\mathbf{s})$ only intersect in $\xi = \mathbf{0}$, then \mathbf{s} is bijective. In a direct optimization of \mathbf{x}_h , above constraint is usually not feasible since for most \mathbf{x}_D , the set $\{\mathbf{x}_h \in \mathcal{V}_h^{\mathbf{x}_D} \mid C^1(\mathbf{x}_h) \cap C^2(\mathbf{x}_h) = \{\mathbf{0}\}\}$ is very small or even empty. However, in the case of optimizing \mathbf{s} , for $\mathbf{s}^0 = \xi$, the cones $C^1(\mathbf{s}^0)$ and $C^2(\mathbf{s}^0)$ are generated by $R^+(1, 0)^T$ and $R^+(0, 1)^T$, respectively. A linear constraint $\mathbf{C}^L(\mathbf{s})$ follows from requiring that $C^1(\mathbf{s})$ and $C^2(\mathbf{s})$ be contained in the cones generated by $\mathbb{R}^+ \times \{(1, -1 + \epsilon)^T, (1, 1 - \epsilon)^T\}$ and $\mathbb{R}^+ \times \{(1, 1 + \epsilon)^T, (-1, 1 - \epsilon)^T\}$, respectively. Here $\epsilon \ll 1$ is a small positive parameter. Clearly, $\mathbf{C}_L(\mathbf{s}^0)$ is located exactly in the center of the feasible region (see Figure 10), making the constraint much less restrictive at the expense of having to compute \mathbf{x}_h^* first.

Remark. We can combine the proposed constraints with the principles from Section 4.1 to suppress overshoots due to extreme diffusive anisotropy. If $\mathbf{C}(\mathbf{s}) = \mathbf{C}_L(\mathbf{s})$, the problem remains convex.

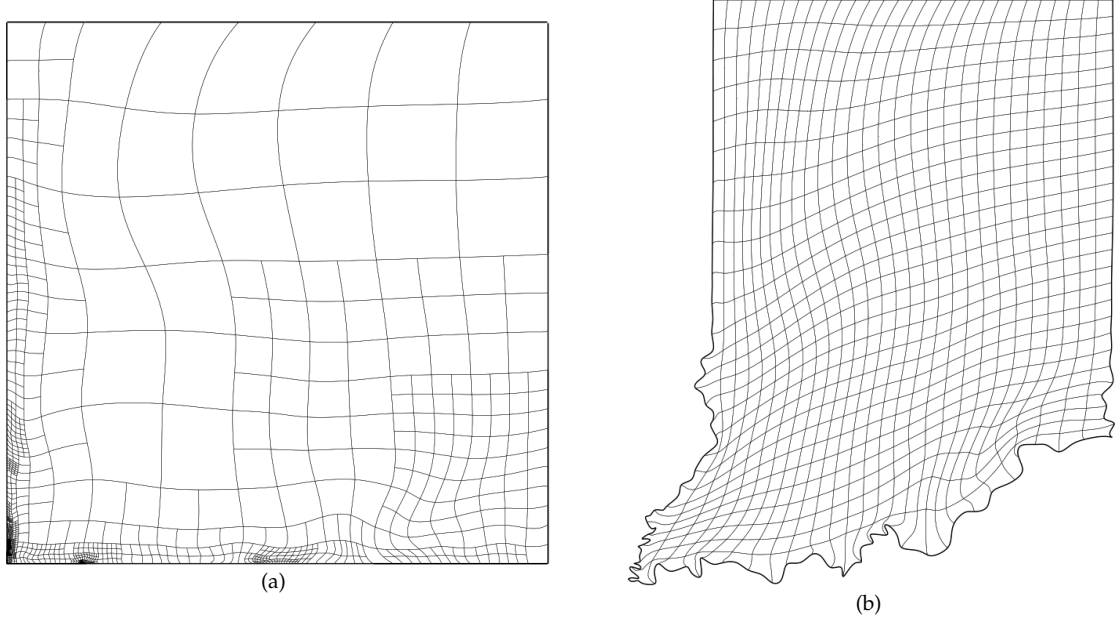


Figure 11: Result of reparameterizing the domain corresponding to the U.S. state of Indiana with $Q = Q^s_{\text{AreaOrthogonality}}$ (a) and the resulting recomputed geometry parameterization (b).

Figure 11(a) shows the domain corresponding to the U.S. state of Indiana (see Figure 4) after optimizing with $Q = Q^s_{\text{AreaOrthogonality}}$ under the constraint $\mathbf{C}(\mathbf{s}) = \hat{\mathbf{d}}(\mathbf{s})$ (see equation (79)). The domain mapping $\mathbf{s}(\xi)$ is built from the same THB-basis as \mathbf{x}_h^* , comprised of 2338 DOFs. Since Newton failed to converge, we recomputed \mathbf{x}_h using the Picard approach, which converged after 21 iterations. The result is depicted in Figure 11. No a posteriori refinements were required. The reparameterization reduces the value of $L_{\text{AreaOrthogonality}}$ from the initial $L_{\text{AreaOrthogonality}}(\mathbf{x}_h^*) = 1.77 \times 10^2$ to $L_{\text{AreaOrthogonality}}(\mathbf{x}_h) = 1.36 \times 10^2$.

Next, we optimize the domain corresponding to the puzzle piece geometry (see Figure 2(b)) with $\mathbf{C}(\mathbf{s}) = \mathbf{C}_L(\mathbf{s})$ and $Q = Q^s_{\text{Area}}$. Hereby, $\mathbf{s}(\xi)$ is built from a structured spline space comprised of 646 DOFs. The reparameterized domain is depicted in Figure 12(a). Bijectivity of \mathbf{x}_h is achieved with 2632 DOFs and the resulting parameterization is depicted in 12(b). With $L_{\text{Area}}(\mathbf{x}_h) = 142.710$, it is roughly as effective as the reparameterization from Figure 7 with $k = 1$.

Figure 13 shows the German province of North Rhine-Westphalia upon reparameterization with $Q = Q^s_{\text{Orthogonality}}$, where $\mathbf{s}(\xi)$ is built from a structured spline space comprised of 578 DOFs, with $\mathbf{C}(\mathbf{s}) = \mathbf{C}_L(\mathbf{s})$. Initially, $L_{\text{Orthogonality}}(\mathbf{x}_h^*) = 18.929$, while $L_{\text{Orthogonality}}(\mathbf{x}_h) = 5.160$ upon recomputation. Bijectivity is achieved with 4584 DOFs, which is roughly double the initial 2724 DOFs.

Finally, Figure 14 shows the result of reparameterizing the same geometry with $Q = Q^s_{\text{AreaOrthogonality}}$ and the same constraints. Initially, $L_{\text{AreaOrthogonality}}(\mathbf{x}_h^*) = 51.244$, while $L_{\text{AreaOrthogonality}}(\mathbf{x}_h) = 30.896$ upon recomputation. Bijectivity is achieved with only 2928 DOFs.

4.3. Direct Approach

As an alternative to optimizing the domain, we may choose to directly optimize the parameterization with respect to a quality cost function. As an advantage, we avoid the (possibly expensive) recomputation of \mathbf{x}_h . In order to avoid folding, constraints should be employed. As a disadvantage, the linear constraint $\mathbf{C}_L(\mathbf{s})$ cannot be used and the initial guess \mathbf{x}_h^* may fail to satisfy the conditions $\hat{\mathbf{d}}(\mathbf{x}_h) > \mathbf{0}$ and $\mathbf{C}_\alpha(\mathbf{x}_h) > \mathbf{0}$ despite being bijective. Heuristically, for complicated geometries, this is usually the case. In such cases, the only viable constraint is $\mathbf{C}^\Xi(\mathbf{s})$.

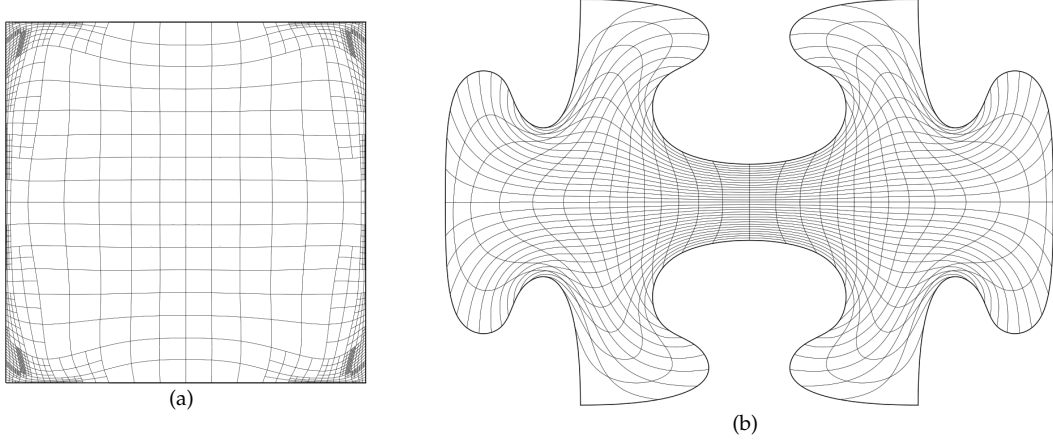


Figure 12: Result of optimizing the puzzle piece domain with $Q = Q_{\text{Area}}^s$ under the constraint $\mathbf{C}(\mathbf{s}) = \mathbf{C}_L(\mathbf{s})$ (a) and the corresponding recomputed mapping (b).

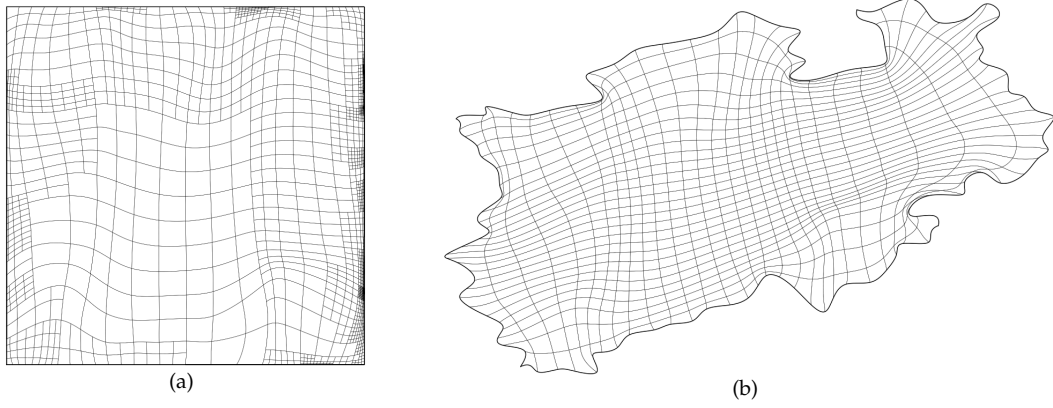


Figure 13: Result of reparameterizing the reference parameterization of the German province of North Rhine-Westphalia (see Figure 5), with $Q(\mathbf{s}) = Q_{\text{Orthogonality}}^s(\mathbf{s})$. The reparameterized domain is shown in (a), while (b) shows the recomputed parameterization.

We optimize the puzzle piece geometry with $Q(\mathbf{x}_h) = Q_{\text{Area}}(\mathbf{x}_h)$ under the constraint $\hat{\mathbf{d}}(\mathbf{x}_h) \geq 0$, where the initial guess \mathbf{x}_h^* is the parameterization from Figure 7(a). Figure 15 shows the resulting parameterization. Convergence is achieved after 21 constrained iterations. The reparameterization reduces L_{Area} from the initial $L_{\text{Area}}(\mathbf{x}_h^*) = 3.29 \times 10^2$ to $L_{\text{Area}}(\mathbf{x}_h) = 0.96 \times 10^2$, which is slightly more pronounced than the reduction from Figure 7 with $k = 1.5$. However, the resulting parameterization is less regular compared to Figure 7(d), which can be remedied by adding a regularization of the form $Q(\mathbf{x}_h) = Q_{\text{Area}}(\mathbf{x}_h) + \beta Q_{\text{Uniformity}}(\mathbf{x}_h)$. Next, we optimize the U.S. state of Indiana with $Q(\mathbf{x}_h) = Q_{\text{Area}}(\mathbf{x}_h)$ under the constraint $\mathbf{C}^\Xi(\mathbf{x}_h) \geq 0$ with

$$\epsilon_i^L = \alpha_L \times \det J(\mathbf{x}_h^*)(\xi_i^c) \quad \text{and} \quad \epsilon_i^U = \alpha_U \times \det J(\mathbf{x}_h^*)(\xi_i^c), \quad (86)$$

(see equation (83)).

Figure 16 shows the resulting parameterization after 30 iterations. With $L_{\text{Area}}(\mathbf{x}_h^*) = 1.049 \times 10^2$ and $L_{\text{Area}}(\mathbf{x}_h) = 0.989 \times 10^2$, the reduction is mild, yet somewhat more pronounced than in Figure 9. Here, Ξ results from uniform sampling with 36 points per element. The choice of the relaxation factors $0 \leq \alpha_L \leq 1$ and $1 \leq \alpha_U$ in (86) tunes to which degree trading an increase in L_{Area} for a decrease in $L_{\text{Orthogonality}}$ is acceptable. Here, more conservative choices lead to less cost function reduction but to more uniform cell sizes and vice

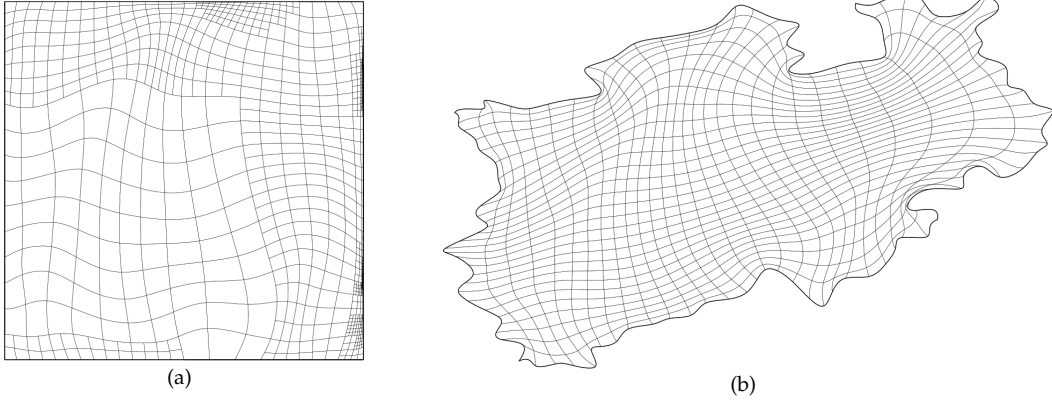


Figure 14: Result of reparameterizing the reference parameterization of the German province of North Rhine-Westphalia (see Figure 5), with $Q(\mathbf{s}) = Q_{\text{AreaOrthogonality}}^{\mathbf{s}}$. The reparameterized domain is shown in (a), while (b) shows the recomputed parameterization.

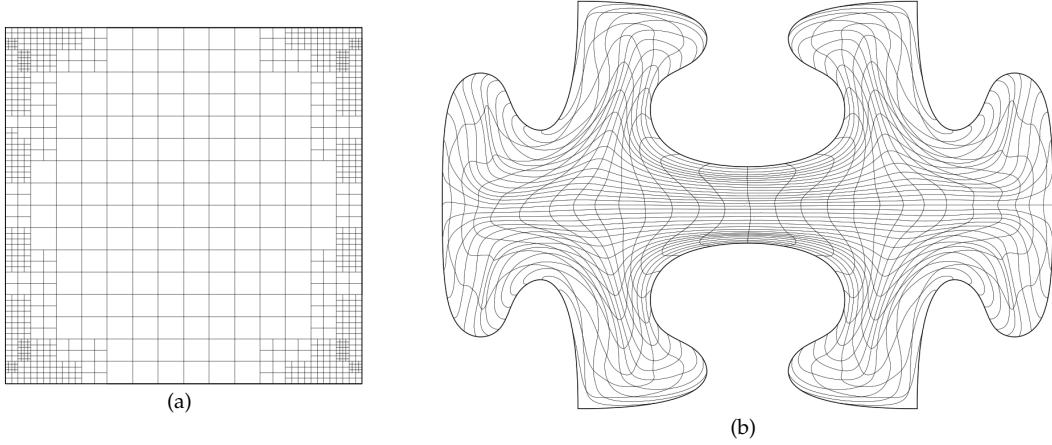


Figure 15: The puzzle piece geometry after 21 iterations of minimizing $Q(\mathbf{x}_h) = Q_{\text{Area}}$ under the constraint $\hat{\mathbf{d}}(\mathbf{x}_h) > 0$ (b) and the corresponding domain (a). The minimization was initialized with the parameterization from Figure 7(a).

versa. Furthermore, values of α_L closer to 1 prevent the grid from folding, even if fewer sampling points are used. We used $\alpha_L = 0.05$ and $\alpha_U = 4$.

4.4. Achieving Boundary Orthogonality

Many applications favor parameterizations with isolines that are orthogonal to the boundary contours. One way to achieve this is allowing $\lambda_i = \lambda_i(\xi)$ in (78) and taking $\lambda_{\text{Orthogonality}}$ large close to $\partial\hat{\Omega}$. We are considering the example of achieving orthogonality at the northern and southern boundaries of the geometry depicted in Figure 17. To this end, we minimize the cost function

$$Q(\mathbf{s}) = (1 + \lambda_{\text{O}}(\xi))Q_{\text{Orthogonality}}^{\mathbf{s}},$$

where $\lambda_{\text{O}}(\xi)$ takes on large values close to the northern and southern boundaries of $\partial\hat{\Omega}$. We employ the constraint $\mathbf{C}(\mathbf{s}) = \mathbf{C}_L(\mathbf{s})$, where $\mathbf{s}(\xi)$ is built from a structured spline space comprised of 594 DOFs. The resulting parameterization is depicted in Figure 18. The figure indeed shows a large degree of orthogonalization, which is somewhat weaker in the protruded parts of the geometry. This is due to orthogonality only being enforced

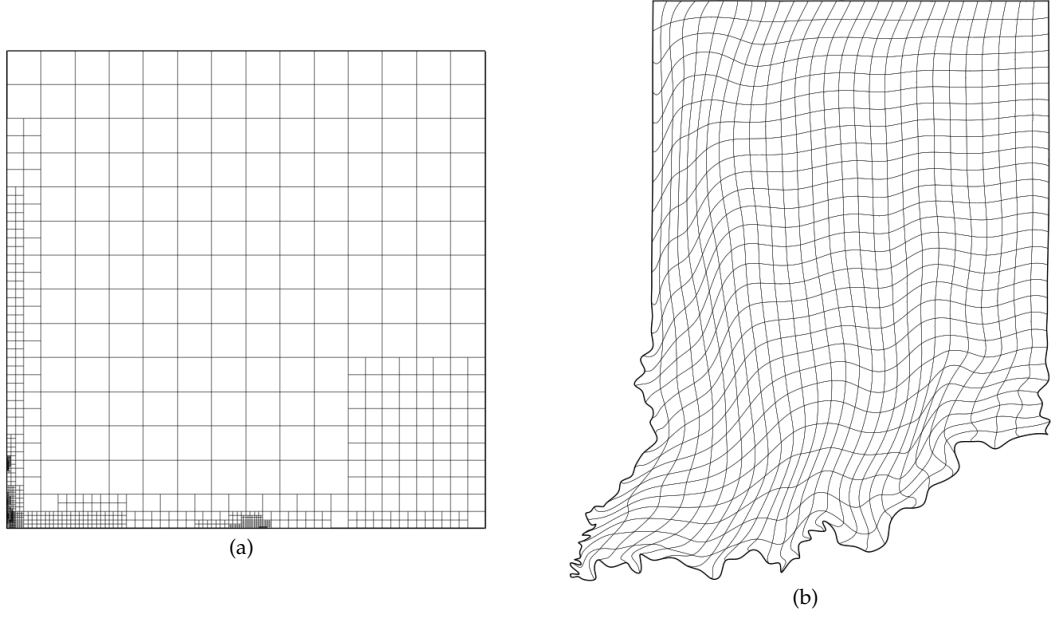


Figure 16: The parameterization of the U.S. state of Indiana after 30 iterations of minimizing $Q(\mathbf{x}_H) = Q_{\text{Area}}$ (b) and the corresponding domain (a). The minimization was initialized with the parameterization from Figure 9(a).

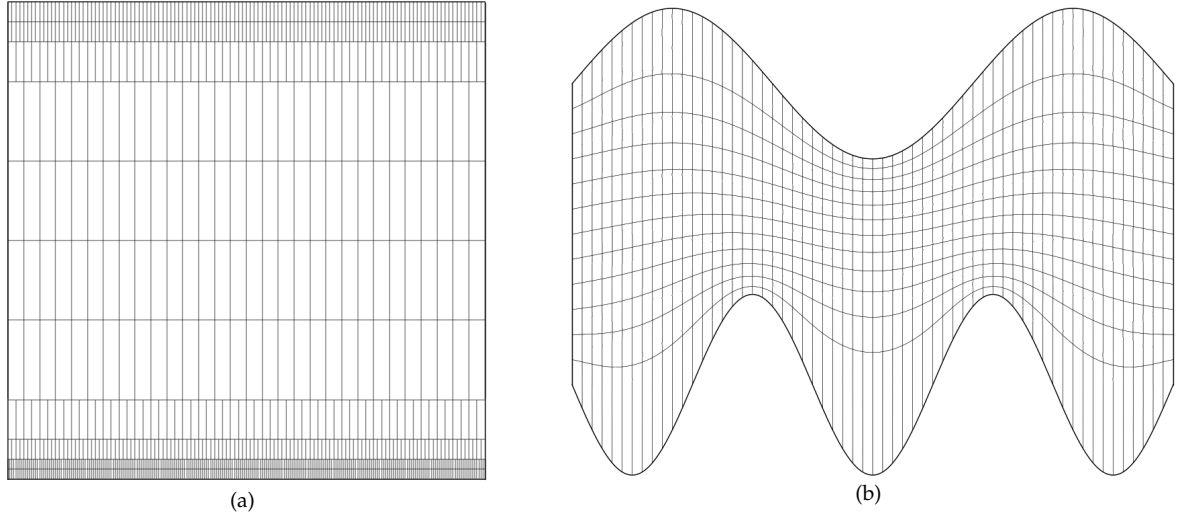


Figure 17: Reference parameterization of a tube-like shaped geometry which is to be orthogonalized by the northern and southern boundaries.

weakly through a penalty term. More pronounced boundary orthogonalization may be achieved by taking λ_O larger close to $\partial\hat{\Omega}$.

Let $\gamma_e, \gamma_w, \gamma_s$ and γ_n refer to the eastern, western, southern and northern parts of $\partial\hat{\Omega}$, respectively. For a more drastic boundary orthogonalization, we follow the approach from [19, Chapter 6], which consists of

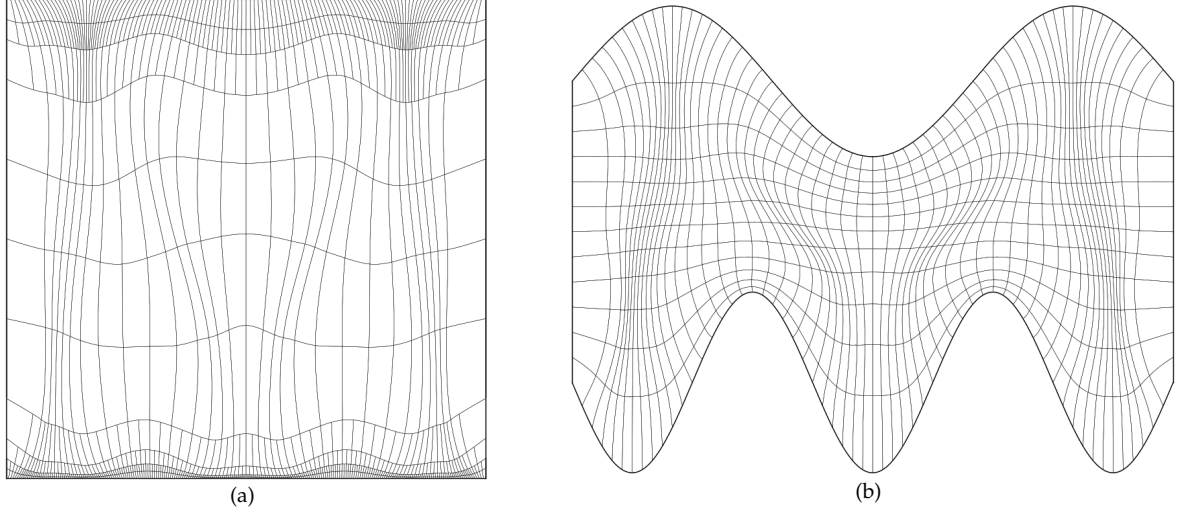


Figure 18: Result of reparameterizing the geometry mapping from Figure 17 by weakly enforcing boundary orthogonality through a large penalty term (b) and the corresponding reparameterized domain (a).

solving the problem

$$\Delta_{\mathbf{x}_h^*} f = 0 \quad \text{s.t.} \quad f = 0 \text{ on } \gamma_e, \quad f = 1 \text{ on } \gamma_w \quad \text{and} \quad \frac{\partial f}{\partial \mathbf{n}} = 0 \text{ on } \gamma_s \cup \gamma_n \quad (87)$$

on an initial folding-free geometry parameterization \mathbf{x}_h^* , where \mathbf{n} denotes the unit outward normal vector on $\partial\Omega$. Upon completion, the control mapping $\mathbf{s} = (s, t)^T$ is computed from

$$s(\xi, \eta) = f(\xi, 0)H_0(\eta) + f(\xi, 1)H_1(\eta) \quad \text{and} \quad t(\xi, \eta) = \eta, \quad (88)$$

where

$$H_0(\eta) = (1 + 2\eta)(1 - \eta)^2 \quad \text{and} \quad H_1(\eta) = (3 - 2\eta)\eta^2 \quad (89)$$

are cubic Hermite interpolation functions. It can be shown that with this choice of s and t , the solution of (64) is orthogonal at γ_s and γ_n . We approximately solve for f by computing the solution f_h of the discretized counterpart of (87) over some structured spline space \mathcal{V}_h . Hereby, the Neumann boundary conditions are weakly imposed through partial integration. The control mapping follows from replacing $f \rightarrow f_h$ in (88). Should orthogonality at γ_w and γ_e be desired, we simply exchange the roles of $s \rightarrow t$, $(\gamma_s, \gamma_n) \rightarrow (\gamma_w, \gamma_e)$ and $\xi \rightarrow \eta$.

Remark. Unlike f , f_h may fail to be monotone increasing on γ_s or γ_n , leading to a folded control mapping $\mathbf{s}(\xi)$.

Figure 19 shows the recomputed parameterization of the same geometry using the preceding methodology, along with the reparameterized domain, which has been computed from the same structured spline basis as in Figure (18). The figure shows an outstanding boundary orthogonalization, which comes at the expense of larger elements in the protruded parts compared to Figure 18. We introduce another control mapping $\mathbf{s}'(\xi)$, which we compute from the solution of

$$\int_{\hat{\Omega}} (\det \partial_s \mathbf{x}_h)^k (g_{11} + \beta g_{22})_{\mathbf{s} \rightarrow \mathbf{s}'} \det \partial_{\xi} \mathbf{s} dS \rightarrow \min_{\mathbf{s}' \in \mathcal{V}_h^2}, \quad \text{s.t.} \quad \mathbf{s}'(\xi) = \mathbf{s}(\xi) \text{ on } \partial\hat{\Omega}, \quad (90)$$

where $\mathbf{s} = (s, t)^T$ and \mathbf{x}_h correspond to Figures 18 (a) and (b), respectively. Here, as before, $k > 0$ tunes to

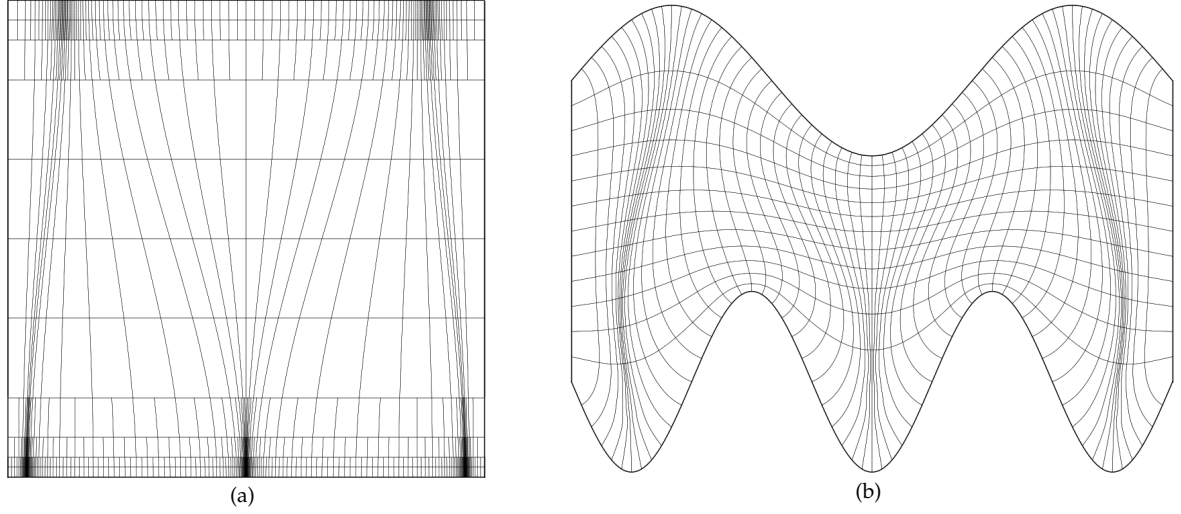


Figure 19: Result of reparameterizing the geometry mapping from Figure 17 using the approach proposed in [19, Chapter 6] (b) and the corresponding reparameterized domain (a).

which degree the spread in cell size is penalized, while $\beta > 1$ tunes the degree to which \mathbf{s}' is contracted / expanded in the direction of $\partial_\eta \mathbf{s}$, in order to compensate for large / small cells in \mathbf{x}_h . Taking β large essentially freezes \mathbf{s}' in the direction of $\partial_\xi \mathbf{s}$, such that boundary orthogonality is preserved. Note that in (90), we are essentially solving the discrete counterpart of

$$\nabla_{\mathbf{s}} \cdot (D \nabla_{\mathbf{s}} \mathbf{s}'_i) = 0, \quad i \in \{1, 2\}, \quad \text{s.t.} \quad \mathbf{s}'(\boldsymbol{\xi}) = \mathbf{s}(\boldsymbol{\xi}), \quad \text{with} \quad D = (\det \partial_{\mathbf{s}} \mathbf{x}_h)^k \begin{pmatrix} 1 & 0 \\ 0 & \beta \end{pmatrix}. \quad (91)$$

Figure 20 shows the geometry parameterization along with the reparameterized domain upon recomputation

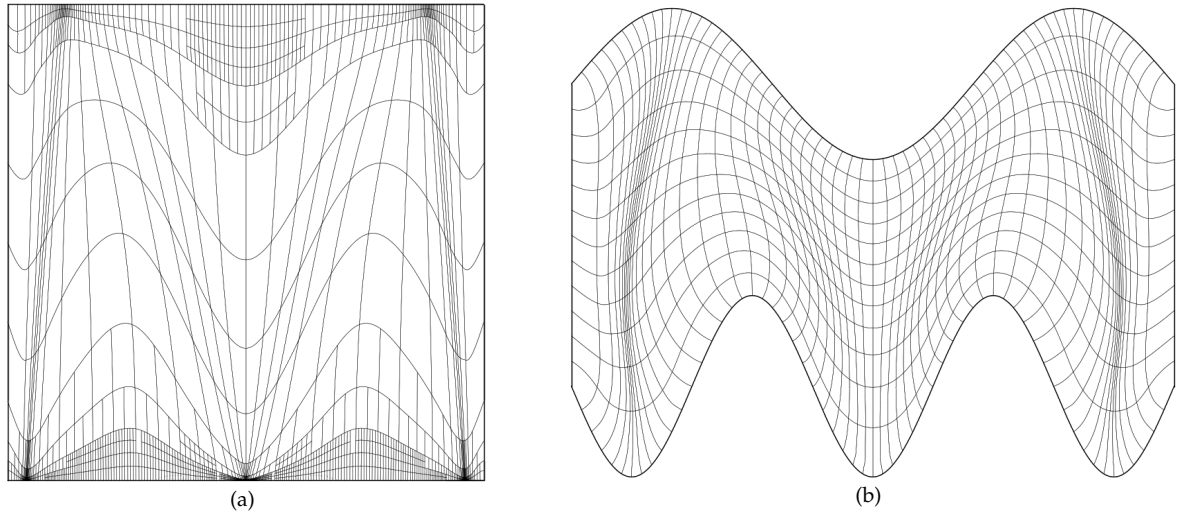


Figure 20: Result of reparameterizing the geometry mapping from Figure 19 using the principles from Section 4.1 (b) and the corresponding reparameterized domain (a).

with $k = 0.75$ and $\beta = 300$. Compared to Figure 19, the figure shows a much better cell size distribution, in

particular close to the boundaries. Large cells can be further penalized by increasing the value of k .

5. Conclusion

In this work, we presented a goal-oriented adaptive THB-spline framework for PDE-based planar parameterization. For this, we adopted the a posteriori refinement technique of dual weighted residual and proposed several goal-oriented refinement cost functions. This resulted in numerical schemes that combine iterative solution techniques with THB-enabled local a posteriori refinement strategies, hence avoiding over-refinement in computing a folding-free geometry parameterization.

In order to fine-tune the parametric properties of the resulting mapping, we combined aforementioned schemes with the concept of domain optimization. Hereby, the (convex) domain which constitutes the target domain of the mapping inverse, is reparameterized in order to alter the parametric properties of the recomputed mapping. For this, we proposed several optimization constraints that avoid the loss of bijectivity.

Acknowledgements

The authors gratefully acknowledge the research funding which was partly provided by the MOTOR project that has received funding from the European Unions Horizon 2020 research and innovation program under grant agreement No 678727.

References

- [1] J. A. Cottrell, T. J. Hughes, Y. Bazilevs, *Isogeometric analysis: toward integration of CAD and FEA*, John Wiley & Sons, 2009.
- [2] G. Xu, B. Mourrain, R. Duvigneau, A. Galligo, Optimal analysis-aware parameterization of computational domain in isogeometric analysis, in: *International Conference on Geometric Modeling and Processing*, Springer, 2010, pp. 236–254.
- [3] C. Giannelli, B. Jüttler, H. Speleers, Thb-splines: The truncated basis for hierarchical splines, *Computer Aided Geometric Design* 29 (7) (2012) 485–498.
- [4] R. Rannacher, Adaptive finite element methods in flow computations, *Recent Advances in Adaptive Computation. Contemporary Mathematics* 383 (2004) 183–176.
- [5] A. Falini, J. Špeh, B. Jüttler, Planar domain parameterization with thb-splines, *Computer Aided Geometric Design* 35 (2015) 95–108.
- [6] A.-V. Vuong, C. Giannelli, B. Jüttler, B. Simeon, A hierarchical approach to adaptive local refinement in isogeometric analysis, *Computer Methods in Applied Mechanics and Engineering* 200 (49–52) (2011) 3554–3567.
- [7] G. Farin, D. Hansford, Discrete coons patches, *Computer Aided Geometric Design* 16 (7) (1999) 691–700.
- [8] J. Gravesen, A. Evgrafov, D.-M. Nguyen, P. Nørtoft, Planar parametrization in isogeometric analysis, in: *International Conference on Mathematical Methods for Curves and Surfaces*, Springer, 2012, pp. 189–212.
- [9] S. Steinberg, *Fundamentals of grid generation*, CRC press, 1993.
- [10] G. Xu, B. Mourrain, R. Duvigneau, A. Galligo, Parameterization of computational domain in isogeometric analysis: methods and comparison, *Computer Methods in Applied Mechanics and Engineering* 200 (23–24) (2011) 2021–2031.
- [11] L. T. Biegler, V. M. Zavala, Large-scale nonlinear programming using ipopt: An integrating framework for enterprise-wide dynamic optimization, *Computers & Chemical Engineering* 33 (3) (2009) 575–582.
- [12] S. Rjasanow, O. Steinbach, *The fast solution of boundary integral equations*, Springer Science & Business Media, 2007.
- [13] S. A. Sauter, C. Schwab, Boundary element methods, in: *Boundary Element Methods*, Springer, 2010, pp. 183–287.
- [14] E. Kreyszig, *Differential Geometry, Differential Geometry*, Dover Publications, 1991.
URL <https://books.google.nl/books?id=P73DrhE9F0QC>
- [15] J. Hinz, M. Möller, C. Vuik, Spline-based parameterization techniques for twin-screw machine geometries, in: *IOP Conference Series: Materials Science and Engineering*, Vol. 425, IOP Publishing, 2018, p. 012030.
- [16] J. Hinz, M. Möller, C. Vuik, Elliptic grid generation techniques in the framework of isogeometric analysis applications, *Computer Aided Geometric Design*.
- [17] D. A. Knoll, D. E. Keyes, Jacobian-free newton–krylov methods: a survey of approaches and applications, *Journal of Computational Physics* 193 (2) (2004) 357–397.
- [18] C. T. Kelley, D. E. Keyes, Convergence analysis of pseudo-transient continuation, *SIAM Journal on Numerical Analysis* 35 (2) (1998) 508–523.
- [19] J. F. Thompson, B. K. Soni, N. P. Weatherill, *Handbook of grid generation*, CRC press, 1998.
- [20] O. Lakkis, T. Pryer, A finite element method for second order nonvariational elliptic problems, *SIAM Journal on Scientific Computing* 33 (2) (2011) 786–801.
- [21] D. Gallistl, Variational formulation and numerical analysis of linear elliptic equations in nondivergence form with cordes coefficients, *SIAM Journal on Numerical Analysis* 55 (2) (2017) 737–757.

- [22] T. Verstraete, L. Müller, J.-D. Müller, Adjoint-based design optimisation of an internal cooling channel u-bend for minimised pressure losses, *International Journal of Turbomachinery, Propulsion and Power* 2 (2) (2017) 10.
- [23] A. Griewank, A. Walther, *Evaluating derivatives: principles and techniques of algorithmic differentiation*, Vol. 105, Siam, 2008.
- [24] Y. Gao, Y. Wu, J. Xia, Automatic differentiation based discrete adjoint method for aerodynamic design optimization on unstructured meshes, *Chinese Journal of Aeronautics* 30 (2) (2017) 611–627.
- [25] T. J. R. Hughes, J. A. Cottrell, Y. Bazilevs, Isogeometric analysis: Cad, finite elements, nurbs, exact geometry and mesh refinement, *cmame* 194 (2005) 4135–4195.
- [26] S. Prudhomme, J. T. Oden, Computable error estimators and adaptive techniques for fluid flow problems, in: *Error estimation and adaptive discretization methods in computational fluid dynamics*, Springer, 2003, pp. 207–268.